NAIST-IS-DD0461014

Doctoral Dissertation

X-ray structural studies of the radixin FERM domain: The interactions with adhesion molecules PSGL-1 and CD43.

Yumiko Takai

February 1, 2007

Department of Bioinformatics and Genomics
Graduate School of Information Science
Nara Institute of Science and Technology

A Doctoral Dissertation
Submitted to the Graduate School of Information Science,
Nara Institute of Science and Technology
In partial fulfillment of the requirements for the degree of
Doctor of Science.

Thesis Committee:

Professor Toshio Hakoshima (Supervisor)
Professor Naotake Ogasawara (Co-supervisor)
Associate Professor Chojiro Kojima (Co-supervisor)

Radixin FERMドメインのX線結晶構造学的研究：接着分子PSGL-1/CD43との相互作用*

高井　友美子

内容梗概

ERM（ezrin/radixin/moesin）タンパク質は細胞膜や細胞膜上の接着分子とアクチンフィラメントとをつなぐ架橋タンパク質であり、N末端に約300残基からなるFERMドメインをもつ。このFERMドメインと相互作用する分子種は多く、相互作用の結果、細胞接着・細胞骨格の制御などが行われる。これまでにFERMドメインは接着分子CD43、CD44、PSGL-1(P-selectin glycoprotein ligand-1)、ICAM-1,2,3などの細胞質ドメインでの直接の相互作用が報告されているが、これら接着分子のFERMドメイン結合領域の相同性は低い。そこで本研究では接着分子PSGL-1、CD43とラデキシンFERMドメインの複合体X線結晶構造解析を行い、接着分子認識の詳細を明らかにした。両分子共にこれまでに報告されているICAM-2の結合様式と似ていたが、ペプチドのC末端側において、ペプチドの構造、FERMドメインの認識に違いが見られた。これらの複合体構造と、他の接着分子のアライメントからFERMドメインの結合モチーフ(R/K)x$_{(3\sim4)}$(Y/L/I)x(V/L)を提案する。また、CD43細胞質ドメインの溶液状態での形質についての分析を行い、特定の構造を形成せず、伸びきったペプチド状のtailとして存在していることを明らかにした。

キーワード

ERMタンパク質、FERMドメイン、CD43、PSGL-1、X線結晶構造解析

*奈良先端科学技術大学院大学情報科学研究科情報生命科学専攻学位論文, NAIST-IS-DD0461014, 2007 年 2 月 1 日.

X-ray structural studies of the radixin FERM domain: Interactions with adhesion molecules CD43 and PSGL-1*

Yumiko Takai

Abstract

Ezrin/radixin/moesin (ERM) proteins possess the conserved N-terminal FERM domain that interacts with membrane-integrated adhesion molecules such as ICAM-2, CD44, CD43 and other signaling proteins. The interactions between the FERM domain and adhesion molecules are important in cell-extracellular matrix adhesion control, cell-cell repulsion and adhesion for cell-cell communication. Interestingly, the cytoplasmic tails of these adhesion molecules display different peptide lengths and the binding sites for ERM proteins exhibit poor sequence homology. In this study, I characterized the CD43 cytoplasmic domain in solution using a variety of physicochemical analyses. The results indicated that no stable secondary structure exists in solution, suggesting that the CD43 cytoplasmic domain exists in an elongated form. I determined the crystal structures of the FERM domain complexed with cytoplasmic peptides of CD43 and PSGL-1 and showed the details of recognition of these adhesion molecules by the radixin FERM domain. I found that the binding modes resemble that of the previously reported ICAM-2 peptide. Some significant differences in peptide recognition by the FERM domain, however, were observed in the C-terminal region of each peptide compared with the FERM-ICAM-2 complex. Based on these findings of our structural studies and sequence comparison with other adhesion molecules that bind ERM proteins, I suggest a more general FERM recognition motif that binds adhesion molecules, (R/K)$x_{(3\sim4)}$(Y/L/I)x(V/L).

Keywords:

ERM protein, FERM domain, CD43, PSGL-1, X-ray crystallography

.*Doctoral Dissertation, Department of Bioinformatics and genomics, Graduate School of Information

Science, Nara Institute of Science and Technology, NAIST-IS-DD0461614, February 1, 2007.

X-ray structural studies of the radixin FERM domain: Interactions with adhesion molecules CD43 and PSGL-1

Abstract

Ezrin/radixin/moesin (ERM) proteins possess the conserved N-terminal FERM domain that interacts with membrane-integrated adhesion molecules such as ICAM-2, CD44, CD43 and other signaling proteins. The interactions between the FERM domain and adhesion molecules are important in cell-extracellular matrix adhesion control, cell-cell repulsion and adhesion for cell-cell communication. Interestingly, the cytoplasmic tails of these adhesion molecules display different peptide lengths and the binding sites for ERM proteins exhibit poor sequence homology. In this study, I characterized the CD43 cytoplasmic domain in solution using a variety of physicochemical analyses. The results indicated that no stable secondary structure exists in solution, suggesting that the CD43 cytoplasmic domain exists in an elongated form. I determined the crystal structures of the FERM domain complexed with cytoplasmic peptides of CD43 and PSGL-1 and showed the details of recognition of these adhesion molecules by the radixin FERM domain. I found that the binding modes resemble that of the previously reported ICAM-2 peptide. Some significant differences in peptide recognition by the FERM domain, however, were observed in the C-terminal region of each peptide compared with the FERM-ICAM-2 complex. Based on these findings of our structural studies and sequence comparison with other adhesion molecules that bind ERM proteins, I suggest a more general FERM recognition motif that binds adhesion molecules, (R/K)$x_{(3\sim4)}$(Y/L/I)x(V/L).

Contents

1 Introduction

1.1 Structure of ERM proteins

The ezrin-radixin-moesin (ERM) family of closely related cytoskeletal proteins provides a regulated linkage between F-actin and membrane-associated proteins (Mangeat et al. 1999; Yonemura et al. 1999; Bretscher et al. 2002). The ERM proteins consist of an N-terminal ~300-residue FERM (four-point one ERM) domain, followed by a ~160-residue region predicted to be largely α-helical, and terminating in a ~90-residue C-terminal tail domain (Figure 1A). FERM (Four-point one, ezrin, radixin, moesin) domains occur in numerous membrane-associated signaling and cytoskeletal proteins to mediate protein-peptide and protein-lipid bindings. Generally located at or near the amino terminus of a protein, they are connected by linkers to various domains. Figure 1B shows a domain map of the FERM superfamily of proteins (Chishti et al. 1998). The sequences of their N-terminal halves are highly conserved (~ 85% identity) and are similar to the N-terminal half of human erythroid band 4.1 protein (~ 78 kDa), indicating that the ERM family is included in the band 4.1 superfamily that includes merlin/schwannomin (a tumor suppressor molecule for neurofibromatosis type II), talin, PTP-H1 and PTP-MEG. Among these, merlin (isoforms I–III) (~ 70 kDa) is fairly similar to the ERM proteins (~ 60% identity) (Shimizu et al. 2002). The FERM domain comprises a membrane-binding site in band 4.1 protein, and similar sequences have recently been found in the central portion of PTPBAS and the C-terminal domain of myosin VIIA (Bretscher et al. 2002). Figure 1A shows a schematic of the radixin FERM domain structure. The globular FERM domain is composed of three subdomains (A, B and C) that are arranged in a clover leaf shape. Although no sequence conservation is evident, all three subdomains possess structural homology to previously described folds (Figure

2A) (Hamada et al. 2000). Subdomain A of radixin (residues 1–82) is very similar to ubiquitin, subdomain B (residues 96–195) has structural similarity to acyl-CoA binding protein and subdomain C (residues 204–297) shows structural homology to an adaptable module that has variously been described as a phosphotyrosine-binding (PTB) or Pleckstrin-homology (PH) domain. This versatile domain has been found to bind peptide and lipid ligands in both signaling and cytoskeletal proteins (Balla 2005).

1.2 Conformational regulation of ERM proteins

ERM proteins exist in two states, a dormant state in which the FERM domain binds to its own C-terminal tail thereby precluding binding to some partner proteins, and an activated state, in which the FERM domain binds to one of many membrane binding proteins and the C-terminal tail binds to F-actin (Figure 3) (Andreoli et al. 1994; Gary and Bretscher 1995; Magendantz et al. 1995).

To date, several structures have been reported including that of a complex between the FERM domain of moesin (residues 1–297) and its C-terminal tail (residues 467–577) (Figure 2B) (Pearson et al. 2000; Li et al. 2007), the FERM domain of radixin (residues 1–310) alone and complexed with inositol trisphosphate (InsP3) (Figure 2A) (Hamada et al. 2000) and the moesin FERM domain with part of the α-helical central domain (residues 1–346) (Edwards and Keep 2001). A comparison of these structures provides the first insight into the FERM domain and how the C-terminal tail domain binds to and modifies the overall structure. ERM proteins are present in the cytosol in an inactive form, in which the adhesion molecule binding site on the N-terminal FERM (4.1 and ERM) domain and the actin filament binding site on the C-terminal tail (C-tail) domain are masked (Figure 2). This inactive form is activated following binding to phosphatidylinositol 4,5-bisphosphate (PIP2) (Hirao et al. 1996) and phosphorylation at

the C-terminal tail domain (T558 in moesin, T564 in radixin) (Matsui et al. 1999). Recent cell biological studies demonstrated that PIP2 binding is the primary requirement in the activation of ERM proteins (Yonemura et al. 2002; Fievet et al. 2004) and at least three kinases (Rho-kinase, Protein kinase Cα and PKCθ) have been shown to phosphorylate the conserved threonine residue in the C-terminal tail domain (Matsui et al. 1998; Pietromonaco et al. 1998; Simons et al. 1998; Tran Quang et al. 2000; Ng et al. 2001). *In vitro* functional analysis suggested that C-terminal threonine phosphorylation maintains ERM proteins in the active state by suppressing the intramolecular interaction (Matsui et al. 1998).

1.3 ERM proteins participate in signaling by Rho

The regulation of ERM protein conformation by a combination of phospholipid binding and phosphorylation has been proposed to lie downstream of the signals mediated by small GTPase, Rho (Kotani et al. 1997; Fukata et al. 1998; Shaw et al. 1998; Matsui et al. 1999) (Figure 3). PIP2-producing phosphatidylinositol 4-phosphate 5-kinase (PI4P5K) has also been reported to be a direct Rho effector (Ren et al. 1996; Ren and Schwartz 1998). Since activation of dormant ERM proteins can be induced by PIP2, one possible pathway for the activation of ERM proteins has been suggested as follows (Tsukita and Yonemura 1999). Rho may activate PI4P5K, which in turn increases the amount of PIP2. PIP2 then activates ERM proteins by inhibiting their interdomain interaction, which allows for phosphorylation of the C-terminal threonine residue by unidentified kinases. On the other hand, immunoprecipitation experiments identified Rho-GDI (GDP dissociation inhibitor) in the CD44-ERM protein complex (Hirao et al. 1996). An *in vitro* binding study then revealed that active but not inactive forms of ERM proteins bind directly to Rho-GDI at their N-terminal halves (Takahashi et al. 1997).

Interestingly, the binding of ERM proteins suppressed the GDI activity of Rho-GDI, whereby GDP-Rho was released from Rho-GDI, and was followed by activation of GTP-Rho possibly through Dbl (GDP/GTP exchange protein) (Takahashi et al. 1997; Takahashi et al. 1998). These findings suggested that ERM proteins, once activated, can activate Rho, which in turn activates ERM proteins as a positive feedback system. In this sense, ERM proteins are located both downstream and upstream of Rho.

1.4 Membrane Binding of ERM Proteins

The N-terminal FERM domain was proposed to interact with membrane proteins on the basis of the membrane-binding properties of the founding FERM family member band 4.1. Two types of interaction with membrane proteins have been documented (Table 1): direct association of the FERM domain with the cytoplasmic tails of transmembrane proteins, and an indirect association with the tail of membrane proteins through two related scaffolding proteins, EBP50/NHE-RF and NHE type 3 kinase A regulatory protein (E3KARP), that contain PDZ domains (Reczek et al. 1997; Reczek and Bretscher 1998; Yun et al. 1998; Terawaki et al. 2006).

1.5 Direct association with membrane proteins.

The cytoplasmic domains of many adhesion molecules are known to play an essential role in adhesive events by serving as sites for structural and functional linkages between cell surface molecules and cytoskeletal components. These interactions are involved in cell-cell and cell-matrix adhesion as well as receptor-ligand interactions, receptor internalization, redistribution, shedding, endocytic sorting and signal transduction. Most of the direct interactions between ERM proteins and transmembrane proteins involve

adhesion molecules (Table 1). The N-terminal halves of ERM proteins were reported to bind directly to the cytoplasmic domains of CD44 (Tsukita et al. 1994; Hirao et al. 1996) and other integral membrane proteins such as ICAM-1, -2 and -3 and CD43, which co-localized with ERM proteins *in vivo* (Yonemura et al. 1993; Tsukita et al. 1994; Helander et al. 1996; Hirao et al. 1996; Serrador et al. 1997; Heiska et al. 1998; Serrador et al. 1998; Yonemura et al. 1998). Although the cytoplasmic domains of these integral membrane proteins display no pronounced shared sequences (Table 2), the juxtamembrane positively charged amino acid clusters are thought to be responsible for binding to ERM proteins (Legg and Isacke 1998; Yonemura et al. 1998). This direct binding of ERM proteins with integral membrane proteins was shown to be essential for cell-surface morphogenesis such as microvillus formation (Yonemura et al. 1999).

Adhesion molecule CD43 and PSGL-1 (P-selectin glycoprotein ligand-1) are expressed on leucocytes and belong to the family of mucin-type molecules (Figure 4). PSGL-1, which is expressed as a homodimer, mediates leukocyte adhesion to endothelial cells and is critically involved in inflammatory responses both in brain and in peripheral tissues by utilizing the interaction of ERM proteins (McEver and Cummings 1997). To date, various membrane proteins that participate in direct linkages to ERM proteins include L1-CAM (Dickson et al. 2002; Haas et al. 2004; Cheng et al. 2005), VCAM-1 (Barreiro et al. 2002), Syndecan-2 (Granes et al. 2003) and NEP (Iwase et al. 2004) (Table 1). A recent crystal structure of the radixin FERM domain complexed with the ICAM-2 cytoplasmic tail revealed that the FERM domain recognizes the signature sequence RxxTYxVxxA (motif-1) (Figure 2C) (Hamada et al. 2001; Hamada et al. 2003).

1.6 Scaffolding protein-mediated membrane protein association.

In addition to associating directly with the cytoplasmic tails of membrane proteins,

the FERM domain interacts strongly with EBP50/NHERF-1 and E3KARP/NHERF-2. Both of these proteins possess two PDZ domains and a C-terminal sequence of 30 amino acids that binds ezrin (Reczek and Bretscher 1998; Yun et al. 1998). PDZ domains typically recognize a specific consensus sequence in the extreme carboxyl terminus of their substrates, and the PDZ domains of EBP50/NHE-RF and E3KARP have been proposed to bind a plethora of membrane and cytoplasmic proteins (Voltz et al. 2001). The crystal structures of the FERM domain bound to NHERF peptides show a new peptide binding site for NHERF peptides that possess a novel signature sequence comprising the sequence MDWxxxxx(L/I)Fxx(L/F) (Motif-2) (Figure 2D) (Terawaki et al. 2006). The Motif-2 amino acid sequence forms an amphipathic α-helix for hydrophobic docking to the groove formed by two ß-sheets from the ß-sandwich of subdomain C. This binding site is distinct from the Motif-1 binding site at the groove formed by strand ß5C and helix α1C. Thus, the FERM domain provides two distinct binding sites for two classes of target proteins with different specificity. Both motif-1 and motif-2 binding interfaces overlap with the C-terminal tail binding region (Figure 2).

1.7 Aim of this study

ICAM-2 possesses a short (18 residues) cytoplasmic tail that strongly binds ERM proteins. In 2003 our laboratory reported a 2.8 Å resolution diffraction analysis of a complex between the radixin N-terminal FERM domain and a 28-residue peptide from the ICAM-2 C-terminal peptide (Hamada et al. 2003). This crystallographic investigation, combined with sequence and structural comparisons, suggested that the FERM domain recognizes the signature sequence RxxTYxVxxA. Although FERM-associated adhesion molecules possess a similar sequence to the ICAM-2 C-terminal region, no adhesion molecules known to date possess a sequence that completely matches the binding motif.

Here I report on the structural studies of CD43 cytoplasmic tail in solution and the 2.9 Å resolution crystallographic structure of a complex comprising the FERM domain and a 20-residue peptide from CD43. I also report the 2.8 Å resolution crystal structure of the radixin N-terminal FERM domain complexed with an 18-residue peptide from the juxtamembrane region of PSGL-1. I showed that CD43 did not form a specific globular structure at the cytoplasmic region, regardless of the longer cytoplasmic region comprising 124 residues in comparison to other adhesion molecules such as ICAM-2 (Figure 4). These crystallographic studies revealed that CD43 and PSGL-1 engage the FERM domain in a very similar fashion to that observed with ICAM-2 binding. Combined with sequence and structural comparisons with ICAM-2 binding, I suggests a more general sequence motif for FERM binding, (R/K)x(3-4)(Y/L/I)x(V/L). Deviations from the ICAM-2 binding features are marked at the region of C terminus of the peptide involved in FERM binding. CD43 and PSGL-1 peptide do not need to form the 3_{10}-helix or ß-turn for binding to the FERM domain.

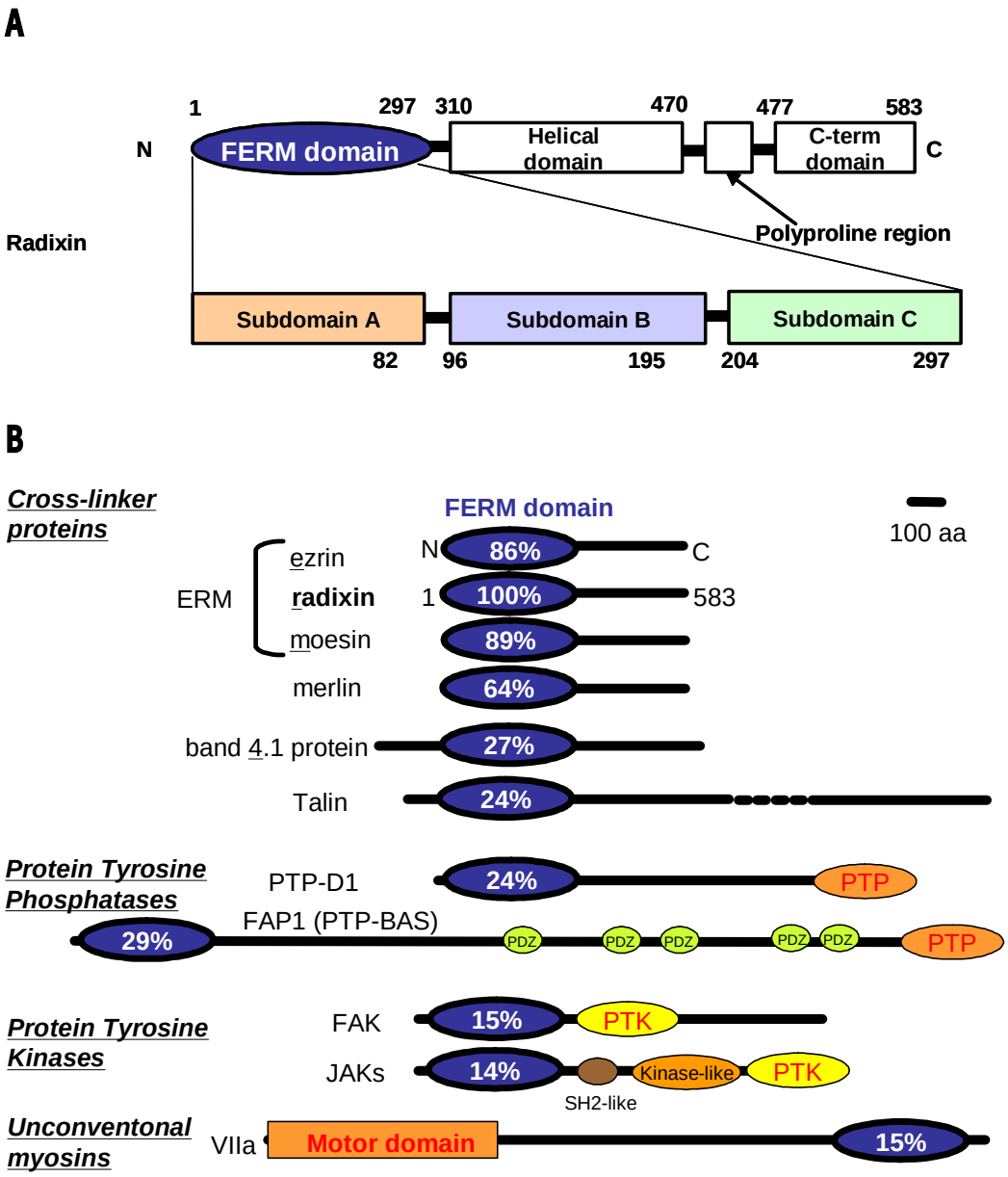

Figure 1 FERM-containing proteins

(A) Diagram of radixin domains. The N-terminal FERM domain (blue), helical domain, polyproline region, and the C-terminal autoinhibitory domain are indicated. Three subdomains in the FERM domain are also indicated, subdomains, A (the N-terminal 82 residues, light yellow), B (residues 96-195, light purple) and C (residues 204-297, light green).
(B) Domain organization of proteins that contain the FERM domain (blue ellipses). Additional domains include the structurally related to the Src-homology-2 domain (SH2-like), tyrosine-kinase domain (PTK), the PSD95-Dlg-ZO1-homology domain (PDZ), the protein-tyrosine-phosphatase domain (PTP) and the myosin subfragment-1 (S-1; Motor domain). The amino acid identity between each FERM domain and the radixin FERM domain is indicated.

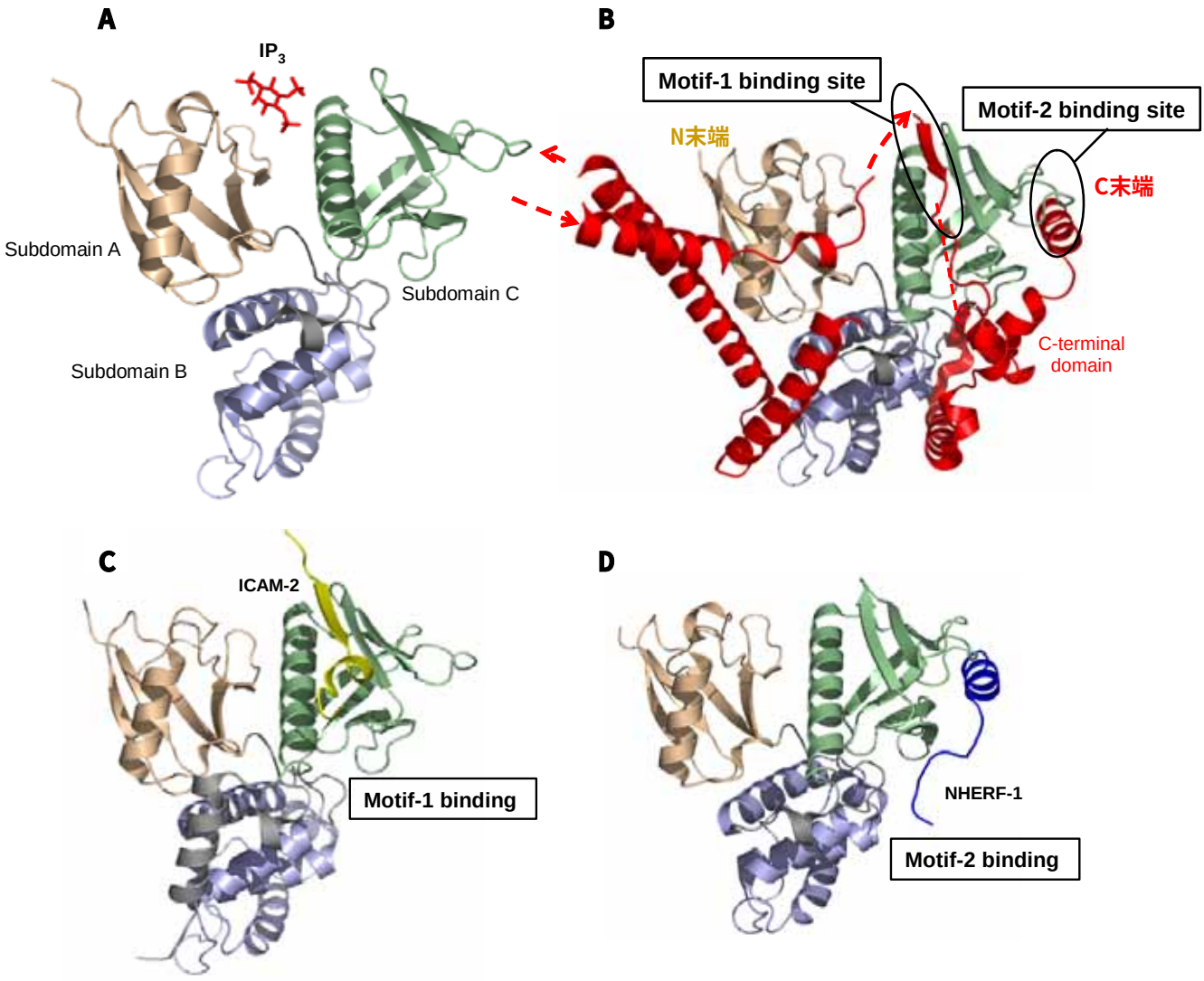

Figure 2 Multi-biding modes found in the FERM domain of ERM proteins

(A) The radixin FERM domain complexed with Ins(1,4,5)P_3 (stick model), subdomain A (wheat), subdomain B (light blue), subdomain C (pale green) (Hamada et al. 2000) PDB accession number 1GC6.
(B) The moesin FERM domain complexed with the C-tail domain (red) (Li et al. 2007)PDB accession number 2i1j.
(C) The radixin FERM domain complexed with the NHERF-1 peptide (blue) (Terawaki et al. 2006) PDB accession number 2D10.
(D) The radixin FERM domain complexed with the ICAM-2 cytoplasmic peptide (yellow) (Hamada et al. 2003) PDB accession number 1J19.

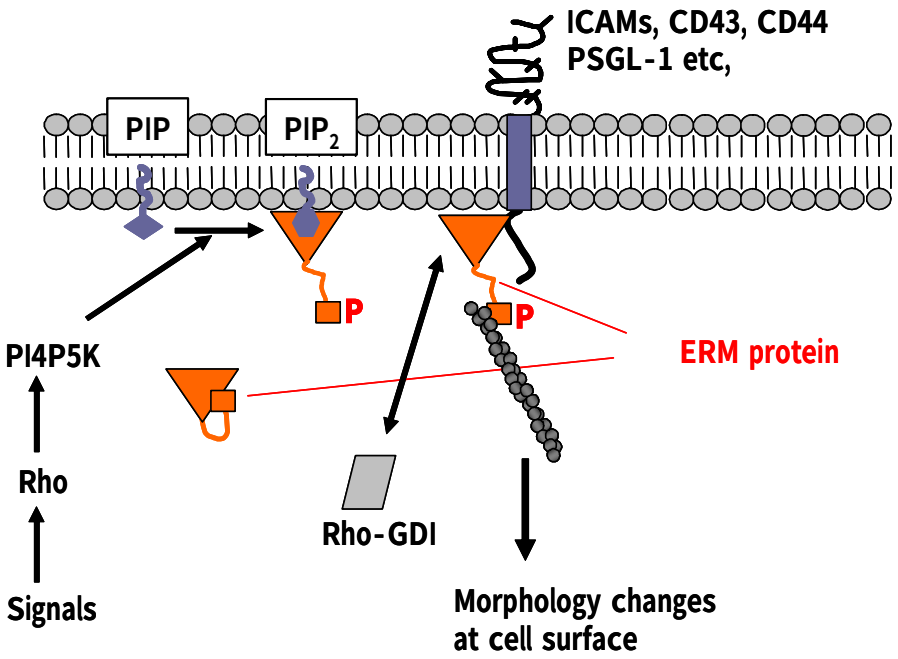

Figure 3 Activation pathway of ERM proteins

Rho activates PI4P5K, which increases the amount of PIP_2. PIP_2 then activates ERM proteins, which allows phosphorylation of their C-terminal threonine residue by some kinases. The C-terminal threonine-phosphorylated ERM proteins are stabilized in the activated forms, which function as actin filament/plasma membrane cross-linkers. Activated ERM proteins are associated directly with the adhesion molecules such as CD44, CD43, and ICAM-1, 2, 3 and PSGL-1. Activated ERM proteins also bind to Rho-GDI at their N-terminal FERM domains, suppressing GDI activity of Rho-GDI to release Rho, which is resulted in activation of Rho. This GTP-bound active Rho can be used to activate ERM proteins just beneath the plasma membranes, providing a positive feedback pathway.

Table 1 ERM-binding partners

	Binding region	Possible role of interaction	Reference
Integral membrane proteins			
ICAM-1	FERM subC	Uropod localization	(1)
ICAM-2	FERM subC	NK cell killing	(2)
ICAM-3	FERM subC	Polarization	(3)
CD44	FERM subC	Uropod localization	(4)
CD43	FERM subC	Immune synapse formation	(5)
CD95	Ezrin FERM	Uropod localization, Apoptosis	(6)
PSGL-1	FERM subC	Rolling, Uropod localization	(7)
L-selectin	FERM subC	Rolling, Microvillar positioning	(8)
Syndecan-2	FERM	Polarization	(9)
NEP	FERM subC	Cell adhesion and migration	(10)
L-1 CAM	FERM	Neuronal development	(11)
VCAM-1	FERM	leukocyte adhesion and transendothelial migration	(12)
Cytosolic proteins			
NHERF-1/EBP50	FERM subC	organizing apical epithelial membranes	(13)
NHERF-2/E3KARP	FERM subC	organizing apical epithelial membranes	(14)
NHE-1	FERM	Regulates the cortical cytoskeleton and cell shape	(15)
SAP97	FERM	Polarized functions in microvilli	(16)
Rho-GDI	FERM subA	Feedback Rho signaling	(17)
Dbl	FERM	Regulate the Rho family members	(18)
FAK	FERM	Trigger FAK activation	(19)
PI3K	FERM	Apoptotic survival	(20)
Hamartin	FERM	Forming focal adhesion	(21)
N-WASP	FERM	Actin Polymerization Function	(22)

The binding partners for the FERM domain of ERM proteins are listed, together with the binding region in the FERM domain and the role of the interaction. ICAM: Intracelluar adhesion molecule, RhoGDI: Rho GDP dissociation inhibitor, Dbl: Diffuse B cell Lymphoma, FAK: Focal adhesion kinase, PI3K: Phosphatidylinositol-3 kinase, N-WASP: Neuronal-Wiskkot Aldrich Syndrome protein, PSGL-1: P-selectin glycoprotein Ligand-1, NEP: Neutral endpeptidase 2.4.11, SAP: Synapse-associated protein 97, EBP50: ERM binding phosphoprotein 50kDa, NHE: Na^{+}/H^{+} exchanger, NHERF: Na^{+}/H^{+} exchange regulatory factor
sub: subdomain

References

(1) Barreiro O, Yanez-Mo M, Serrador JM, Montoya MC, Vicente-Manzanares M, Tejedor R, Furthmayr H, Sanchez-Madrid F.
Dynamic interaction of VCAM-1 and ICAM-1 with moesin and ezrin in a novel endothelial docking structure for adherent leukocytes.
J Cell Biol. 2002 Jun 24;157(7):1233-45.

(2) Yonemura S, Hirao M, Doi Y, Takahashi N, Kondo T, Tsukita S, Tsukita S.
Ezrin/radixin/moesin (ERM) proteins bind to a positively charged amino acid cluster in the juxta-membrane cytoplasmic domain of CD44, CD43, and ICAM-2.

J Cell Biol. 1998 Feb 23;140(4):885-95.
(3) Serrador JM, Alonso-Lebrero JL, del Pozo MA, Furthmayr H, Schwartz-Albiez R, Calvo J, Lozano F, Sanchez-Madrid F.
Moesin interacts with the cytoplasmic region of intercellular adhesion molecule-3 and is redistributed to the uropod of T lymphocytes during cell polarization.
J Cell Biol. 1997 Sep 22;138(6):1409-23.
(4) Tsukita S, Oishi K, Sato N, Sagara J, Kawai A, Tsukita S.
ERM family members as molecular linkers between the cell surface glycoprotein CD44 and actin-based cytoskeletons.
J Cell Biol. 1994 Jul;126(2):391-401.
(5) Yonemura S, Hirao M, Doi Y, Takahashi N, Kondo T, Tsukita S, Tsukita S.
Ezrin/radixin/moesin (ERM) proteins bind to a positively charged amino acid cluster in the juxta-membrane cytoplasmic domain of CD44, CD43, and ICAM-2.
J Cell Biol. 1998 Feb 23;140(4):885-95.
(6) Parlato S, Giammarioli AM, Logozzi M, Lozupone F, Matarrese P, Luciani F, Falchi M, Malorni W, Fais S.
CD95 (APO-1/Fas) linkage to the actin cytoskeleton through ezrin in human T lymphocytes: a novel regulatory mechanism of the CD95 apoptotic pathway.
EMBO J. 2000 Oct 2;19(19):5123-34.
Lozupone F, Lugini L, Matarrese P, Luciani F, Federici C, Iessi E, Margutti P, Stassi G, Malorni W, Fais S.
Identification and relevance of the CD95-binding domain in the N-terminal region of ezrin.
J Biol Chem. 2004 Mar 5;279(10):9199-207. Epub 2003 Dec 15.
(7) Snapp KR, Heitzig CE, Kansas GS.
Attachment of the PSGL-1 cytoplasmic domain to the actin cytoskeleton is essential for leukocyte rolling on P-selectin.
Blood. 2002 Jun 15;99(12):4494-502.
Serrador JM, Urzainqui A, Alonso-Lebrero JL, Cabrero JR, Montoya MC, Vicente-Manzanares M, Yanez-Mo M, Sanchez-Madrid F.
A juxta-membrane amino acid sequence of P-selectin glycoprotein ligand-1 is involved in moesin binding and ezrin/radixin/moesin-directed targeting at the trailing edge of migrating lymphocytes.
Eur J Immunol. 2002 Jun;32(6):1560-6.
(8) Ivetic A, Deka J, Ridley A, Ager A.
The cytoplasmic tail of L-selectin interacts with members of the Ezrin-Radixin-Moesin (ERM) family of proteins: cell activation-dependent binding of Moesin but not Ezrin.
J Biol Chem. 2002 Jan 18;277(3):2321-9. Epub 2001 Nov 8.
Ivetic A, Florey O, Deka J, Haskard DO, Ager A, Ridley AJ. Related Articles, Links
Mutagenesis of the ezrin-radixin-moesin binding domain of L-selectin tail affects shedding, microvillar positioning, and leukocyte tethering.
J Biol Chem. 2004 Aug 6;279(32):33263-72. Epub 2004 Jun 3.
(9) Berndt C, Roy C, Mangeat P, Reina M, Vilaro S.
Identification of a novel Ezrin-binding site in syndecan-2 cytoplasmic domain.Granes F,
FEBS Lett. 2003 Jul 17;547(1-3):212-6.
(10) Iwase A, Shen R, Navarro D, Nanus DM.
Direct binding of neutral endopeptidase 24.11 to ezrin/radixin/moesin (ERM) proteins competes with the interaction of CD44 with ERM proteins.
J Biol Chem. 2004 Mar 19;279(12):11898-905. Epub 2004 Jan 2.
(11) Dickson TC, Mintz CD, Benson DL, Salton SR.
Functional binding interaction identified between the axonal CAM L1 and members of the ERM family.
J Cell Biol. 2002 Jun 24;157(7):1105-12. Epub 2002 Jun 17.
(12) Olga Barreiro, María Yáñez-Mó, Juan M. Serrador, María C. Montoya, Miguel Vicente-Manzanares, Reyes Tejedor, Heinz Furthmayr, and Francisco Sánchez-Madrid
Dynamic interaction of VCAM-1 and ICAM-1 with moesin and ezrin in a novel endothelial docking structure for adherent leukocytes
The Journal of Cell Biology, Volume 157, Number 7, June 24, 2002 1233–1245
(13) Reczek D, Berryman M, Bretscher A.
Identification of EBP50: A PDZ-containing phosphoprotein that associates with members of the ezrin-radixin-moesin family.
J Cell Biol. 1997 Oct 6;139(1):169-79.
(14) Yun CH, Lamprecht G, Forster DV, Sidor A.

NHE3 kinase A regulatory protein E3KARP binds the epithelial brush border Na+/H+ exchanger NHE3 and the cytoskeletal protein ezrin.
J Biol Chem. 1998 Oct 2;273(40):25856-63.
(15) Denker SP, Huang DC, Orlowski J, Furthmayr H, Barber DL.
Direct binding of the Na--H exchanger NHE1 to ERM proteins regulates the cortical cytoskeleton and cell shape independently of H(+) translocation.
Mol Cell. 2000 Dec;6(6):1425-36.
(16) Bonilha VL, Rodriguez-Boulan E.
Polarity and developmental regulation of two PDZ proteins in the retinal pigment epithelium.
Invest Ophthalmol Vis Sci. 2001 Dec;42(13):3274-82.
(17) Takahashi K, Sasaki T, Mammoto A, Takaishi K, Kameyama T, Tsukita S, Takai Y.
Direct interaction of the Rho GDP dissociation inhibitor with ezrin/radixin/moesin initiates the activation of the Rho small G protein.
J Biol Chem. 1997 Sep 12;272(37):23371-5.
(18) Takahashi K, Sasaki T, Mammoto A, Hotta I, Takaishi K, Imamura H, Nakano K, Kodama A, Takai Y.
Interaction of radixin with Rho small G protein GDP/GTP exchange protein Dbl.
Oncogene. 1998 Jun 25;16(25):3279-84.
(19) Poullet P, Gautreau A, Kadare G, Girault JA, Louvard D, Arpin M.
Ezrin interacts with focal adhesion kinase and induces its activation independently of cell-matrix adhesion.
J Biol Chem. 2001 Oct 5;276(40):37686-91. Epub 2001 Jul 23.
(20) Gautreau A, Poullet P, Louvard D, Arpin M.
Ezrin, a plasma membrane-microfilament linker, signals cell survival through the phosphatidylinositol 3-kinase/Akt pathway.
Proc Natl Acad Sci U S A. 1999 Jun 22;96(13):7300-5.
(21) Lamb RF, Roy C, Diefenbach TJ, Vinters HV, Johnson MW, Jay DG, Hall A.
The TSC1 tumour suppressor hamartin regulates cell adhesion through ERM proteins and the GTPase Rho.
Nat Cell Biol. 2000 May;2(5):281-7.
(22) MF, Gusella JF, Ramesh N, Snapper SB, Ramesh V.
The NF2 tumor suppressor Merlin and the ERM proteins interact with N-WASP and regulate its actin polymerization function.Manchanda N, Lyubimova A, Ho HY, James
J Biol Chem. 2005 Apr 1;280(13):12517-22. Epub 2005 Feb 7.

Table 2 Sequence alignment of the juxtamembrane cytoplasmic regions of adhesion molecules that bind ERM proteins

hCD43	276		R	R	R	Q	K	R	R	T	G	A	L	V	L	S	R	G	G	K	R	N
mCD43	272		R	Q	R	Q	K	R	R	T	G	A	L	T	L	S	G	G	G	K	R	N
rCD43	255		R	Q	R	Q	K	R	R	T	G	A	L	T	L	S	R	G	G	K	R	N
hPSGL-1	342		A	V	R	L	S	R	K	G	H	M	Y	P	V	R	N	Y	S	P	T	E
mPSGL-1	329		A	V	R	L	S	R	K	T	H	M	Y	P	V	R	N	Y	S	P	T	E
hICAM-2	249	G	Q	H	L	R	Q	Q	R	M	G	T	Y	G	V	R	A	A	W	R	R	L
mICAM-2	248	G	Q	H	W	H	R	R	R	T	G	T	Y	G	V	L	A	A	W	R	R	L
hICAM-1	504				N	R	Q	R	K	I	K	K	Y	R	L	Q	Q	A	Q	K	G	T
mICAM-1	510				N	R	Q	R	K	I	R	I	Y	K	L	Q	K	A	Q	E	E	A
hICAM-3	511				R	E	H	Q	R	S	G	S	Y	H	V	R	E	E	S	T	Y	L
hCD44	671	N	S	R	R	R	C	G	Q	K	K	K	L	V	I	N	S	G	N	G	A	V
mCD44	707	N	S	R	R	R	C	G	Q	K	K	K	L	V	I	N	G	G	N	G	T	V
hL1	1144					K	R	S	K	G	G	K	Y	S	V	K	D	K	E	D	T	Q
mL1	1147					K	R	S	K	G	G	K	Y	S	V	K	D	K	E	D	T	Q
hSyndecan-2	170			R	M	R	K	K	D	E	G	S	Y	D	L	G	E	R	K	P	S	S
mSyndecan-2	171			R	M	R	K	K	D	E	G	S	Y	D	L	G	E	R	K	P	S	S
mVCAM-1	721				R	K	A	N	M	K	G	S	Y	S	L	V	E	A	Q	K	S	K
rVCAM-1	721				R	K	A	N	M	K	G	S	Y	S	L	V	E	A	Q	K	S	K

hCD43	G	V	V	D	A	W	A	G	P	A	Q	V	P	E	E	G	A	V	T	V	T	376
mCD43	G	V	V	D	A	W	A	G	P	A	R	V	P	D	E	E	A	T	T	T	S	312
rCD43	G	T	V	D	A	W	A	G	P	A	R	V	P	D	E	E	A	T	T	A	S	295
hPSGL-1	M	V	C	I	S	S	L	L	P	D	G	G	E	G	P	S	A	T	A	N	G	382
mPSGL-1	M	I	C	I	S	S	L	L	P	E	G	G	D	G	A	P	V	T	A	N	G	369
hICAM-2	P	Q	A	F	R	P																275
mICAM-2	P	R	A	F	R	A	R	P	V													277
hICAM-1	P	M	K	P	N	T	Q	A	T	P	P											532
mICAM-1	I	K	L	K	G	Q	A	P	P	P												537
hICAM-3	P	L	T	S	M	Q	P	T	E	A	M	G	E	E	P	S	R	A	E			547
hCD44	E	D	R	K	P	S	G	L	N	G	E	A	S	K	S	Q	E	M	V	H	L	711
mCD44	E	D	R	K	P	S	E	L	N	G	E	A	S	K	S	Q	E	M	V	H	L	748
hL1	V	D	S	E	A	R	P	M	K	D	E	T	F	G	E	Y	R	S	L	E	S	1181
mL1	V	D	S	E	A	R	P	M	K	D	E	T	F	G	E	Y	R	S	L	E	S	1184
hSyndecan-2	A	A	Y	Q	K	A	P	T	K	E	F	Y	A									201
mSyndecan-2	A	A	Y	Q	K	A	P	T	K	E	F	Y	A									202
mVCAM-1	V																					739
rVCAM-1	V																					739

Basic and acidic residues are shown in blue and red, respectively. Key residues of the ICAM-2 peptide for binding to the radixin FERM domain are shown in green and residues that correspond to key residues of ICAM-2binding to the FERM domain are highlighted in gray. The sources are mouse (m), rat (r), and human (h). The residue numbers for N- and C-terminal residues are shown.

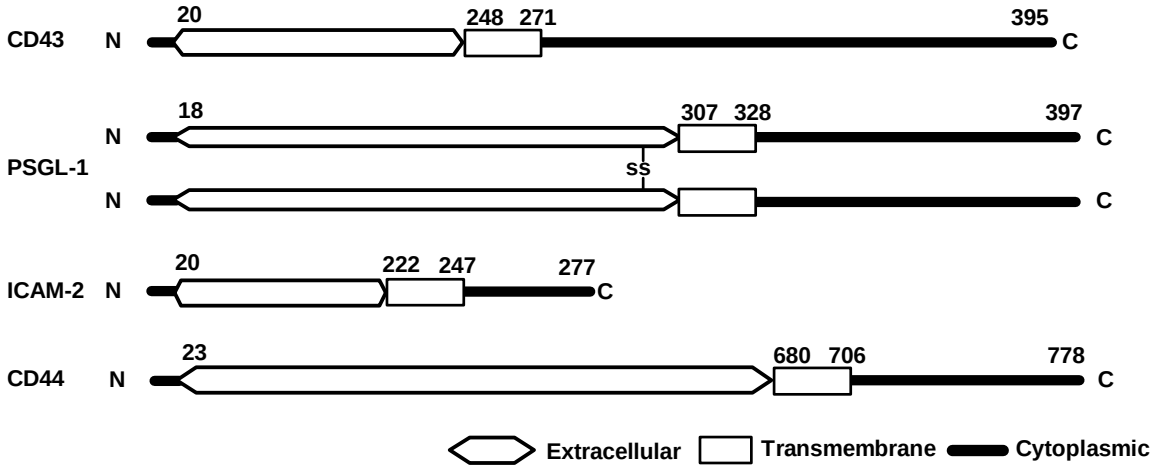

Figure 4 The domain structure of mouse adhesion molecules that bind to ERM proteins

ICAM-2 (mouse 277 residues) consists of two immunoglobulin fold domains in the extracellular part, a transmembrane helix and the cytosolic tail of 28 residues. CD43 (395 residues) has the cytoplasmic domain consisting of 124 residues and an extracellular domain highly modified with sialomutin containing surfars. PSGL-1 is also sialomutin family adhesion molecule and the cytoplasmic domain consisting of 69 residues. PSGL-1 forms homodimer at extracellular domain. CD44 (778 residues) has the cytoplasmic domain consisting of 70 residues and an extracellular hyaluronic acid receptor. All these adhesion molecules are single-pass type1 membrane protein.

2 Materials and methods

2.1 Protein preparation

The FERM domain (residues 1-310) of mouse radixin was expressed as a fusion protein with GST in *Escherichia coli* and purified by previously described methods (Hamada et al. 2001). Purification of the rat CD43 cytoplasmic domain was according to the method of Yonemura and Tsukita (Yonemura et al. 1998). Synthesis of the GST fusion proteins was induced by incubating bacteria with 1 mM isopropyl ß-D-thiogalactopyranoside for 2–5 h at 37°C. Cells were sedimented by centrifugation and the resultant cell pellet was solubilized in buffer A (20 mM Tris buffer, pH 8.0, 200 mM NaCl, 1 mM EDTA, 1 mM DTT, 1.5% Sarkosyl, 1 mM PMSF and 20 mg/ml leupeptin) at 4°C. Following sonication, the cell debris was removed by centrifugation (35,000 rpm, 30 min, at 4°C). The supernatant was applied to a GST affinity column comprising glutathione Sepharose 4B (GE Healthcare Bio-Sciences, USA) that had been washed with buffer B (20 mM Tris buffer, pH 8.0, 150 mM NaCl, 1 mM EDTA and 1 mM DTT) and then eluted with buffer B containing 50mM glutathione. The eluted protein was purified by passage through HiTrap Q (GE Healthcare Bio-Sciences, USA) and the GST tag was cleaved following digestion with 5 units ml-1 human thrombin (Sigma-Aldrich, USA) for 5 h at 10°C. The cleaved proteins were collected and further purified by passage through HiTrap SP and HiLoad 16/60 Superdex 75 (GE Healthcare Bio-Sciences, USA). The SDS-PAGE of purified fractions is shown in (Figure 5). The purified protein was concentrated to 13 mg ml^{-1} using Amicon Ultra-15 (Amicon, Beverly, MA, USA). The purified protein was verified with matrix-assisted laser desorption/ionization time-of-flight mass spectroscopy (MALDI-TOF MS; PerSeptive Inc.) and Amino-terminal analysis (M492; Applied Biosystems).

2.2 Biophysical characterization of CD43

For circular dichroism (CD) spectroscopy, protein samples were prepared with 50mM Tris-HCl. Reducing buffer conditions were obtained by supplementing samples with 1mM 2-Mercaptoethanol and 50mM KCl. Far-UV CD spectra were recorded on a J-720W spectropolarimeter (Jasco Inc.) equipped with a quartz cell with 0.1 cm path length. The spectra shown represent the averages of four measurements. Data were evaluated using Jasco (Jasco Inc.) software.

Analytical ultracentrifugation (AUC) was performed on an Optima XL-A analytical ultracentrifuge (Beckman Instruments) equipped with an An-60ti rotor. Recombinant CD43 molecules were analyzed in Tris buffer and protein concentrations were adjusted to 0.5–1.5 mg/ml in Tris-HCl supplemented with 1mM DTT and 100mM KCl. Sedimentation velocity experiments were performed at 40000 r.p.m. in a 12 mm epon double-sector cell at 10°C. Velocity scans were analyzed with the program Sedfit (version 8.7) (Schuck 2000) using 300 scans collected approximately 2 min apart. Size distributions were determined for a confidence level of p = 0.68, a resolution of n = 100, and sedimentation coefficients between 0.1 and 20 s. Sedimentation equilibrium runs were conducted at three protein concentrations performed at 39,000. The molecular weight (MW) was analyzed on the basis of a single species using Beckman software provided as an add-on to Origin Version 4.1 (Microcal Inc.), for which the partial specific volume $\bar{\nu}$ for CD43 was calculated to be 0.711 ml/g from its amino acid and carbohydrate content as determined from its sequence (Perkins 1986).

The molecular size of the native recombinant CD43 cytoplasmic domain was determined using gravity flow gel filtration techniques. CD43 was chromatographed at 4°C through Superose12 HR 10/30 column (GE Healthcare Bio-Sciences, USA) using

buffer containing 20 mM Tris (pH 8.0), 150 mM KCl, 1 mM EDTA and 1 mM DTT. The molecular mass was determined on the basis of the elution volume from a plot of log (molecular mass) of a standard protein versus the elution volume.

2.3 The binding study

In vitro binding was investigated with SPR measurements carried out on a BIAcore Biosensor instrument (Biacore 3000, Biacore). Biotinylated polypeptides of the juxtamembrane region of the adhesion molecules, which were synthesized by an Fmoc-based strategy with standard side-chain protecting groups and purified by reverse phase HPLC, were purchased from Toray Research Center (Tokyo, Japan). The peptide region employed in the binding assay and crystallization were determined according to previous studies concerning CD43 (Yonemura et al. 1998) and PSGL-1 (Urzainqui et al. 2002). The peptide was coupled via the N-terminal biotin moiety to a streptavidin-coated sensor chip (sensor chip SA, Biacore). The radixin FERM domain (~0.1mM) was injected into both the peptide-linked and non-linked sensor chips for correction of background signals. All binding experiments were performed at 25°C with a flow rate of 10 ml/min in buffer comprising 10 mM HEPES (pH 7.4), 150 mM NaCl, 1 mM EDTA, 1 mM DTT and 0.05% surfactant P20. Kinetic parameters were evaluated using the BIA evaluation software (Biacore). K_d values were obtained by averaging of at least three independent measurements and are summarized in (Table 3). GST-fusion full-length CD43 was covalently bound to the sensor chip (sensor chip CM5, Biacore) surface via dextran carboxyl moieties using a GST Kit for fusion capture (Biacore) and then similarly analyzed.

2.4 Crystallization

For crystallization of the FERM domain complexed with CD43, the purified radixin FERM domain (1mM) was mixed with the 20-residue CD43 peptide (5mM) at a 1:1 volume ratio (mol ratio, protein:peptide=1:5). The final protein concentration was 24.6 mg/ml. Crystals of the complex were obtained from a solution containing 100 mM Citrate-Na (pH 5.6), 10% polyethylene glycol 4000 (PEG4K) and 10% (v/v) isopropanol at 4°C. In the case of the FERM domain complexed with PSGL-1, the purified radixin FERM domain (1 mM) was mixed with the 18-residue PSGL-1 peptide (10mM) at a 1:1 volume ratio (mol ratio, protein:peptide=1:10). The final protein concentration was 31 mg/ml. Crystals of the complex were obtained from a solution containing 100 mM Tris-HCl (pH 8.2) and 8% polyethylene glycol 8000 (PEG8K) at 4°C.

All diffraction data were collected from crystals flash-frozen to 100 K following cryoprotection in a solution containing 11% PEG4K, 18% (v/v) iso-propanol, 15% PEG200 and 100 mM Citrate-Na buffer (the FERM-CD43 complex) or 8% PEG8K, 100mM Tris buffer, 20% PEG400 (the FERM-PSGL-1 complex). Crystals of the FERM-CD43 complex belonged to space group $P4_322$, while those of the FERM-PSGL-1 complex belonged to space group $P2_12_12_1$ as determined by the following structure analysis.

2.5 X-ray data collection

Intensity data sets of the FERM-CD43 complex were collected at beam line BL44XU at the SPring-8 synchrotron facility, Harima, Japan. The wavelength was set to 0.9 Å with a crystal-to-detector distance of 600 mm. Data were collected with angular ranges of 180° with step sizes of 3° and an exposure time of 30 s. The crystallographic data and intensity data-processing statistics are summarized in Table 4 and Table 5. The total

number of observed reflections was 90,704 and included 11,007 unique reflections. The resulting data gave an R_{merge} of 12.1% (37.7% for the outer shell, 2.8-2.7 Å) and a completeness of 96.5% (76.4% for the outer shell). The mean I/σ was 7.7 (1.7 for the outer shell) (Table 5).

Intensity data sets of the FERM-PSGL-1 complex were collected at beam line BL41XU at the SPring-8 synchrotron facility, Harima, Japan. The wavelength was set to 1.00 Å with a crystal-to-detector distance of 170 mm. Data were collected from two crystals with angular ranges of 180° with step sizes of 1° and an exposure time of 7 s. Two data sets were merged into one set of data for structure determination. The crystallographic data and intensity data-processing statistics are summarized in Table 4 and Table 5. The total number of observed reflections was 191,709 and included 20,429 unique reflections. The resulting data gave an R_{merge} of 7.1% (11.7% for the outer shell from 2.9 Å to 2.8 Å) with a completeness of 98.4% (92.3% for the outer shell). The mean I/σ was 9.2 (3.7 for the outer shell) (Table 5).

All intensity data were processed using the programs DENZO and SCALEPACK (Otwinowski 1997).

2.6 Structure determination and refinement

The crystal structures of the FERM-CD43 and FERM-PSGL-1 complexes were determined by molecular replacement using the program Molrep in the CCP4 program suite (1994) with the ICAM-2- bound structure of the radixin FERM domain (PDB accession code 1J19), as a search model. The solutions were estimated by *R*-factor (*R*) and Correlation coefficient (*C*). *R* is calculated according to equation 2.1 which represents the sum of the absolute difference between observed $|F_{obs}|$ and calculated $|F_{cal}|$ over the sum of $|F_{obs}|$. *C* is expressed according to equation 2.2. The advantage in using this

value over R is that it is scale insensitive. The solution that possesses a low value of R and a high value of C represents the most agreeable solution (Table 6).

$$R = \frac{\sum_{hkl} (|F_{obs}| - \kappa |F_{calc}|)}{\sum_{hkl} |F_{obs}|} \quad (2.1)$$

$$C = \frac{\sum_{hkl} (|F_{obs}|^2 - \overline{|F_{obs}|^2}) \times (|F_{calc}|^2 - \overline{|F_{calc}|^2})}{\left[\sum_{hkl} (|F_{obs}|^2 - \overline{|F_{obs}|^2})^2 \sum_{hkl} (|F_{calc}|^2 - \overline{|F_{calc}|^2})\right]^{\frac{1}{2}}} \quad (2.2)$$

Initial refinement was performed with CNS (Jones 1991; Brunger et al. 1998) using a rigid-body, simulated annealing, and individual B factor refinement. The resultant initial map showed clear electron densities for most of the FERM domain and the peptide. An initial model of the peptide was built into the electron density map using the graphics program O (Jones 1991) in addition to rebuilding part of the FERM domain.

Figures were generated using PyMOL (http://www.pymol.org DeLano, 2002a). A schematic diagram of the interactions was prepared with the program LIGPLOT.

2.7 Structural comparison of the FERM domain

Structural studies of the FERM domain of other proteins and complexes with adhesion molecules such as ICAM-2 or membrane component Ins(1,4,5)P3 have been reported (Hamada et al. 2001; Hamada et al. 2003). Comparison of our complex structure with these structures shows how the interaction with CD43 or PSGL-1 induces structural changes. Superposition of the FERM domains was carried out using LSQKAB, 1994 CCP4 program suits).

3 Results

3.1 Physicochemical properties of the CD43 cytoplasmic tail in solution

The CD43 cytoplasmic tail consists of 124 amino acids and is relatively large in comparison with ICAM-2 (28 amino acids) or PSGL-1 (69 amino acids). Consequently, it is assumed that the CD43 cytoplasmic tail possesses a stable conformation that may be functionally significant by affecting its interactions with other molecules. Various analyses of the CD43 cytoplasmic tail peptide were conducted in an effort to acquire relevant structural information. Gel filtration analysis was employed to estimate the molecular weight in solution. Passage through Superose 12 HR yielded a single peak that corresponded to a size of 32 kDa, which is ca. 2.5-fold larger than the theoretical molecular weight of 13 kDa, suggesting that the native protein might exist as a dimer or trimer (Figure 6A). Further insight into the secondary structure was gleaned by investigating the circular dichroism spectrum (CD spectrum) of the CD43 cytoplasmic tail. Figure 6B shows that none of the spectra indicate the presence of a helix at a sample concentration 9.7 μM, and it was known that the CD43 cytoplasmic tail formed mostly random coils as determined by secondary structural content analysis which yielded the following content; helix: 0.0%, β-sheet: 18.2%, turn: 29.8%, random: 52%. Furthermore, typical peaks that represent the presence of a stable globular protein molecule were not observed by NMR (Figure 6C). Finally, analytical ultracentrifugation employing both sedimentation velocity and sedimentation equilibrium methods was applied in an effort to investigate the molecular weight of sample in solution, the approximate shape of the molecule and whether it forms a dimer. Sedimentation velocity measurements were performed at a CD43 (cytoplasmic tail peptide) concentration of 1.4 mg/ml and 40000 rpm for 33 hours. The results yielded a single peak at 1 S which suggests the presence of

a monomer, and no peaks to indicate the presence of oligomeric forms (Figure 6D-1). The molecular mass that was calculated from Rmsd (0.088), frictional ratio (2.03) and sedimentation coefficient (1.00) was 16,858 Da and is similar to the theoretical value (13,089). In this analysis, it was demonstrated that the CD43 cytoplasmic tail existed in monomeric form and adopted an extremely elongated shape as estimated from the frictional ratio. Sedimentation equilibrium analysis was also conducted at three different protein concentrations and analyzed at 30,000 and 39,000 rpm. Best fit conditions were achieved at 1.4 mg/ml protein and 39,000 rpm (Figure 6D-2). This analysis was resulted in 12 kDa for the CD43 tail peptide. Therefore, both methods indicated the presence of a monomeric protein.

It was clearly shown that the CD43 cytoplasmic domain exists in monomeric form and adopts an elongated shape with no secondary structure. Most adhesion molecules possess short cytoplasmic tails comprising tens of residues, while CD43 possesses a long cytoplasmic tail comprising 124 residues with no clearly defined folded structure.

3.2 Structural determination and overall structure of the radixin FERM domain and adhesion molecule complexes

The FERM domain (residues 2-310) employed in this study was derived from the mouse radixin FERM domain. Initially, although the full-length CD43 cytoplasmic region was used for the crystallization of the CD43 and radixin FERM domains, these crystallization trials were unsuccessful, probably due to the flexible nature in solution as discussed above. The interaction region of CD43 to the FERM domain has been reported (Yonemura et al. 1998). Consequently, we used short synthetic peptides that include the basic amino acid cluster located in the juxtamembrane region. Quantitative analysis of peptide binding to the radixin FERM domain was performed to determine peptide length

by surface plasmon resonance measurements using a BIAcore Biosensor instrument. The CD43 peptide, which consists of 20 N-terminal residues of the cytoplasmic domain (272 RQRQKRRTGALTLSGGGKRN 291) encompassing the reported binding region, binds the radixin FERM domain with a dissociation constant (K_d) of 1.96 μM (Table 3). This binding affinity is comparable to that of the full-length cytoplasmic domain region (5.27 μM). The peptide regions of PSGL-1 for binding assay and crystallization were determined according to the previous study (Urzainqui et al. 2002). The PSGL-1 peptide of the juxtamembrane region, which consists of 18 N-terminal residues of the PSGL-1 cytoplasmic tail (331 RLSRKTHMYPVRNYSPTE 348), binds to the radixin FERM domain with K_d of 201 nM, and was not significantly different in comparison with the binding affinity of a longer PSGL-1 peptide comprising 32 residues (K_d = 350 nM) (Table 3). From these results, 20 residues of the CD43 peptide (272-291) and 18 residues of the PSGL-1 peptide (331-348) were used for the crystallization (Figure 7).

The FERM-CD43 complex crystals (Figure 8A) were found to belong to space group $P4_322$, with unit-cell parameters $a = b = 68.72$, $c = 201.39$ Å. MALDI-TOF MS of dissolved crystals gave peaks for 37,921.3 Da (calculated mass 37,919 Da of the radixin FERM domain) and 2,240.6 Da (calculated 2,240.5 Da of the CD43 peptide), indicating that the crystals contain both the protein and peptide. A Matthews coefficient (Matthews 1968) of 3.0 $Å^3$ Da^{-1} was calculated assuming the presence of one radixin FERM molecule in the asymmetric unit, which corresponds to 58.1% solvent content by volume. The crystallographic data and intensity data-processing statistics are summarized in Tables 4 and 5.

The FERM-PSGL-1 complex crystals (Figure 8B) were found to belong to space group $P2_12_12_1$, with unit-cell parameters $a = 80.74$, $b = 85.73$, $c = 117.75$ Å. MALDI-TOF MS of dissolved crystals gave peaks for 37,920.7 Da (37,919 Da calculated from the radixin FERM domain) and 2460.4 Da (2,461.8 Da calculated from the PSGL-1 peptide),

indicating that the crystals contain both the protein and peptide. Assuming the presence of two 1:1 FERM-PSGL-1 complexes in the asymmetric unit, a Matthews coefficient of 2.5 $Å^3$ Da^{-1} was calculated assuming the presence of two radixin FERM molecules in the asymmetric unit, which corresponds to 50.9% solvent content by volume. Calculation of the self-rotation map did not yield a peak in the $\kappa = 180°$ section, which suggests that the dimer is not associated with local two-fold symmetry or is associated with a non-crystallographic two-fold axis that is parallel to the crystallographic 2_1 axis.

Both of the structures were determined by molecular replacement using radixin FERM domain bound to ICAM-2 (Hamada et al., 2003). Following several cycles of rebuilding and refinement, the model of the FERM-CD43 complex was refined to an R value of 24.29% (a free R value of 25.53%) for intensity data at 2.9 Å resolution. The refinement statistics are summarized in Table 5. The current model includes 316 residues of the protein (six residues arising from the vector) and 15 residues of the peptide. The stereochemical quality of the model was monitored using the program PROCHECK (Laskowski 1993). In the CD43 peptide model, side chains Lys4, Arg5, Lys17 and Arg18 were poorly defined and in the current structure were replaced with alanines (Figures 7 and 9). No model was built for four N-terminal and one C-terminal residues, which were poorly defined in the current map. As defined in PROCHECK, there were no residues in disallowed main-chain torsion angle regions (Figure 10.1).

Similarly, the model of the FERM-PSGL-1 complex was refined to an R value of 23.17% (a free R value of 29.08%) for intensity data at 2.8 Å resolution. The current structure of the FERM/PSGL-1 complex includes 626 residues of the FERM domain (1-313: A, 1-313: B, three C-terminal residues arising from the vector) and 33 residues of the PSGL-1 (2-17: C, 2-18: D) peptide. The stereochemical quality of the model was monitored using the program PROCHECK. No model of the PSGL-1 peptide for two C-terminal residues (residues 18 and 19) of chain C or for one C-terminal residue of chain

D, which were poorly defined in the current map. In the protein model, no model was built for three C-terminal residues of ether chain A or B, which were poorly defined in the current map (Figures 7 and 9). As defined in PROCHECK, there were no residues in disallowed main-chain torsion angle regions (Figure 10.2).

3.2 Overall structure of radixin FERM domain complexes

The structure of the radixin FERM domain complexes were essentially the same as the reported structures of the free, IP3-bound and ICAM-2-bound forms. The binding sites of the adhesion molecules were also the same as that of ICAM-2 (Figure 11). The FERM domain in the PSGL-1-bound form was most similar to the free form as determined from pair-wise superposition of the overall structure where the root-mean-square (r.m.s) deviations in Cα- carbon atoms was 0.771 Å (Table 7). On the other hand, The FERM domain in the CD43-bound form was most similar to the ICAM-2-bound form where the overall root-mean-square (r.m.s) deviation was 0.637 Å (Table 7). Although the FERM domain forms a stable structure with association of the three subdomains, the domain possesses slight mobility in the A-B and B-C linker regions. Consequently, differences in the overall structures are dependent on the torsion of the A-B linker and vary among the three FERM domains that bind to each adhesion molecule. These differences may be due to crystal packing. Structural similarity among the subdomains that do not possess linker regions was much higher (Table 7). In particular, the structures of subdomain C binding to PSGL-1 or CD43 were very similar to the binding to ICAM-2 (0.483 Å: PSGL-1, 0.379 Å: CD43, Table 7). However, the conformational changes in the FERM domains are quite small and probably are not induced by binding to adhesion molecules.

3.3 Adhesion molecule recognition by the FERM domain

Both binding sites of CD43 and PSGL-1 in the radixin FERM domain were overlapped with that for ICAM-2, where the adhesion molecule peptides fit into the hydrophobic groove formed by helix α1C and strand β5C in subdomain C (Figure 12). Subdomain C consists of two antiparallel β sheets composed of four and three β-strands, respectively, packed into a β-sandwich enclosing a hydrophobic core and a single α-helix at the C terminus packed between strands β5C and β1C (Figure 11). The adhesion molecule peptide was located between helix α1C and strand β5C and forms the additional β-strand next to strand β5 from the β-sheet consisting of β5-β6-β7 (Figure 13). Eight residues of the CD43 or PSGL-1 peptides contact subdomain C, and where the contact areas were 621 Å^2 (CD43) and 1,240 Å^2 (PSGL-1), respectively (ICAM-2 is 1,761 Å^2 with 11 residues). A previous report showed that some adhesion molecules that interact with the FERM domain possess a characteristic sequence that includes the hydrophobic region between polar regions consisting of a basic amino acid cluster at the juxtamembrane. CD43 and PSGL-1 possess hydrophobic regions comprising M9-V12 (4 residues) and G8-G16 (9 residues) and M9-V12 (4 residues), respectively (Figure 7). In this hydrophobic region, adhesion molecules were fixed to subdomain C by forming an antiparallel β sheet with β5C. ICAM-2 forms a β strand with 4 residues (7-10) and a 3_{10}-helix (12-15) follows. On the other hand, CD43 and PSGL-1 formed a β-strand with 4 residues (8-11) given the absence of a 3_{10}-helix. Both CD43 and PSGL-1 are involved in 5 or 6 hydrogen bonds that are utilized in the formation of a β-strand with the main chain (Figures 13 and 17). PSGL-1 residues comprising the β-strand sequence possess relatively large side chains, so that sequence similarity of the PSGL-1 β-strand is low in comparison with other peptides. However, the interaction that forms the β-strand was essentially the same as that for ICAM-2, with the side chain of H8 (G8 of ICAM-2) and

M9 (T9 of ICAM-2) making contact with FERM domain residues (Figure 17). Although the seventh position of all three adhesion molecules is occupied by threonone (Thr7), only Thr7 of ICAM-2 represented the start point of hydrogen bond formation to main-chain atoms from the ß-strand (T7 in Figures 14 and 17). In both CD43 and PSGL-1, Thr7 is located at a position which precludes hydrogen bond formation with the main chain, but allows for hydrogen bond formation to the side chains. Hydrogen bond distances to the side chain were 2.88 Å (CD43) and 2.92 Å (PSGL-1) (Figure 14). Although Thr7 is located at this position in all three molecules, Thr7 does not seem to play an important role for determining binding specificity. Thr7 in human PSGL-1 is occupied by Gly while that in human ICAM-2 is occupied by Met, and is not highly conserved among adhesion molecules (Table 2).

3.4 The N-terminal positively charged region of adhesion molecules

The N-terminal region of adhesion molecules is rich in positively charged amino acids and in ICAM-2, CD43 and PSGL-1 is represented by regions HWHRRR, RQRQKRR and RLSRK, respectively (Table 2). Although it has been suggested that these regions play an important role in the FERM domain interaction *in vivo* (Yonemura et al. 1998), in our analysis, there was no interaction with these positively charged amino acids except for Arg6 (CD43) and Arg5 (PSGL-1). Arg6 and Arg5 interact with Leu274 of helix α1C and Asp252 of strand ß5C, respectively. Arg6 of ICAM-2 also forms a hydrogen bond with Asp252 and hydrophobic interactions with Leu274. Arg6 of CD43 is located in the same position of ICAM-2 so that the interaction is the same, although the density of Asp252 was weak. Arg5 of PSGL-1 does not form a hydrogen bond as is the case with ICAM-2 and CD43 but participates in hydrophobic interactions with Leu274 and Asp252 (Figures 14 and 17). In this region, the side chains of other positively charged amino acids were

disordered or the model was not able to be built (Figures 9 and 14). Therefore it was shown that the N-terminal positively charged amino acid rich regions do not possess clearly defined structure. In the ICAM-2 binding motif RxxTYxxA, Arg6 (ICAM-2 and CD43) corresponds to the first residue. CD43 possesses this motif although PSGL-1 has lysine at the 6 position and arginine at the 5 position. With PSGL-1, Lys6 seems to be involved in the interaction in lieu of the arginie residue, but in fact, the three residues Arg5, Lys6 and Thr7 were slightly compacted and consequently Arg5 engages in weak hydrophobic interactions with Asp252 and Leu274, so that Arg5 of PSGL-1 plays a role similar to Arg6 of ICAM-2 (Figures 14 and 17). It is also believed that the interaction in this N-terminal region precludes tight binding since there is no cluster of negatively charged amino acids in the FERM domain site (Figure 12). These observations show that the N-terminal positively charged amino acid cluster does not represent the FERM domain interaction region and that the arginine residue of the ICAM-2 binding motif is less restricted. It is believed that FERM interaction is practical when the peptide sequence is adapted to Rx(2~3)TYxVxxA.

3.5 Hydrophobic core region of the peptide for FERM interaction

The region of the peptide structure that was well-defined was the hydrophobic region and CD43 and PSGL-1 is represented by regions GALTL (residues 8-12) and HMYPV (8-12), respectively. In the ICAM-2 peptide, Tyr10, Val12 and Ala15 fit deeply in the contact groove, and this hydrophobic region mediates the binding specificity by through contacts of Tyr10 and Val12 with multiple residues of the FERM domain. In particular, Tyr10 forms a hydrogen bond (2.7 Å) with His288 of helix α1C and is highly conserved among species (Table 2). Additionally, mutation analyses of ICAM-2 have shown that this residue is important. The corresponding sequence in PSGL-1 is the same as ICAM-2.

Tyr10 of PSGL-1 also formed a hydrogen bond with His288 of helix α1C (2.7 Å) and makes contact with both Leu281 and Met285 of strand β5C (Figures 15 and 17). CD43 possesses Leu10 and Leu12 corresponding to ICAM-2 Tyr10 and Val12, respectively. These two leucine residues are very important for FERM binding. Leu10 of CD43 makes contact with Ile248, Leu281and Met285 of the FERM domain, and forms the same interaction as Tyr10 of ICAM-2 except for the absence of a hydrogen bond to the His288 in side chain (Figures 15 and 17). In the case of ICAM-2, Val12 includes part of the 3_{10}-helix although CD43 and PSGL-1 do not have a 3_{10}-helix in the corresponding peptide region. However both Leu12 (CD43) and Val12 (PSGL-1) seemed to fit in the same position as Val12 of ICAM-2 and participate in hydrophobic interactions with multiple side chains on the FERM domain so that they play the same role as ICAM-2 residues (Figure 16). It seems that other similar residues such as leucine or isoleucine can contribute toward hydrophobic interactions in lieu of Val12. In fact, the 12 position is occupied with these residues among the different species of ICAM-2 (Table 2). From these results, it became clear that sequences such as CD43 and PSGL-1 corresponded to the FERM domain binding motif of ICAM-2 RxxTYxVxxA, and that the two hydrophobic residues corresponding to Tyr10 and Val12 represented important elements that play a central binding role involved in hydrophobic interactions. Furthermore, it was revealed that residues Tyr10 and Val12 could be substituted for leucine from the structure of the FERM-CD43 complex so that the previous binding motif could be extended and be represented by Rx(3~4)(Y/L)x(V/L).

3.6 The relationship between peptide structures bound to FERM subdomain C and the canonical PTB domain

The C-terminal FERM-binding region of the ICAM-2 peptide forms a 3_{10}-helix

following the ß-strand although CD43 and PSGL-1 have no characteristic structure in this region (Figure 11). It has been known that the structure of FERM subdomain C resembles the PTB domain. Peptides that are recognized by the PTB domain include the NPxY (where Y is usually phosphorylated) motif and usually bind to the PTB domain between an α-helix and a neighboring ß-strand. For example, it has been observed that for the insulin receptor substrate 1 (IRS-1) PTB domain and insulin receptor peptide complex, the NPx(p)Y motif is located on a ß-turn following a short ß-strand and is the region responsible for imparting the binding specificity to the PTB domain (Figure 18A) (Eck et al. 1996). It was reported that the integrin ß3 tail interacting with the talin FERM domain also binds PTB-like subdomain in a manner similar to subdomain C of ERM proteins, and that its binding pattern is dependent on the NPxY motif as is the case with the canonical PTB domain (Figure 18B) (Garcia-Alvarez et al. 2003). Hamada *et al.* showed that the 3_{10}-helix following a short ß-strand participated in the binding of ICAM-2 to the FERM domain (Figure 18D). Thus the presence of a 3_{10}-helix was estimated to be a common structural element structure as reflected in the peptides that bind to the PTB domain or Talin FERM domain. However, hydrogen bonds involved in formation of a 3_{10}-helix and ß-turn were not observed in the peptide structures of CD43 and PSGL-1 (Figures 18E, F). Interactions to FERM subdomain C at this C-terminal region were not observed. The last residue in the FERM binding motif of ICAM-2 RxxTYxVxxA is alanine and contributes toward formation of the 3_{10}-helix mentioned above. Our complexed structures showed that CD43 and PSGL-1 had neither the equivalent residue to alanine nor any interacting residue. Therefore, the first 7 residues in the motif RX(3~4)Y/LXV/L are more important in CD43 and PSGL-1, and the final 3 residues of the ICAM-2 motif, xxA, are not required.

4 Discussions

4.1 The FERM binding motif of adhesion molecules

The ERM protein family consists of proteins known to bind the cytoplasmic tails of several adhesion molecules such as CD44, ICAM-1, -2 and -3 and CD43, however the binding sequence motif common in all the adhesion molecules had not been defined. Adhesion molecules known to bind to the FERM domain include L-selectin (Ivetic et al. 2002), NEP (Neprilysin) (Iwase et al. 2004) and CD95 (Lozupone et al. 2004), in addition to those molecules listed in Table 2. Since many adhesion molecules that interact with the FERM domain possess a positively charged amino acid cluster located at the juxtamembrane region that is believed to be important for mediating the binding interactions observed. The structure of the radixin FERM domain complexed with ICAM-2 showed that FERM domain residues mediating the direct interaction were located within the hydrophobic region following the positively charged amino acid cluster and that the binding was maintained hydrophobic interactions. Alignment of the adhesion molecules on the basis of the interaction features described above fails to yield the presence of a common region corresponding to the FERM domain binding motif of ICAM-2 represented by RxxTYxVxxA. This study revealed that the expanded binding motif Rx(3~4)Y/LxY/L was adaptable. Consequently, the adhesion molecules listed in Table 2 may bind to the FERM domain in a similar manner as the $Rx_{(3\sim4)}$Y/LxV/L motif. CD44 is the representative molecule that interacts with the FERM domain, and possesses isoleucine at position Y/L when aligned with the Rx(3~4)Y/LxV/L motif. Since it is likely that isoleucine can fit into the hydrophobic pocket given its similarity to leucine, the binding motif could be represented as comprising Rx(3~4)Y/L/IxV/L. Using this motif, the alignment of adhesion molecules is shown in Table 2, and from this we

propose that the binding motif comprises R/Kx(3~4)Y/L/IxV/L. Although structural analysis of CD44 has yet to be reported, it is highly anticipated given its low sequence homology. Since L-selectin (RRLKKGKKSQERMDDPY, mouse cytoplasmic tail) possesses neither a hydrophobic region following the positively charged amino acid cluster nor the FERM binding motif, a novel binding site motif that differs from previously determined binding sites may emerge.

The adhesion molecules detailed in this study are all type I transmembrane adhesion molecules (the N-terminus is extracellular, while the C-terminus is cytoplasmic) and type II adhesion molecule NEP (the C-terminus is extracellular, while the N-terminus is cytoplasmic) can interact with the FERM domain. Recent work by Terawaki detailed the binding manner of NEP to the radixin FERM domain and key residues involved in the binding were identified as comprising the QxxxTxI sequence. Residue changes comprising Q to R, T to Y/L/I and I to L/I constitute the FERM binding motif. From these results, if the binding sequence is comprised of RxxTYxVxxA (ICAM-2), RxxxxYxV (PSGL-1), RxxxLxL (CD43) or QxxxTxI, all of these can bind to the FERM domain at precisely the same position. The amino acid selectivity at the 5 or 6 position is low, which is apparent from the complexed structures. The important residues are located at positions 10 and 12, and if position 10 is occupied by Y/I/L/T and position 12 by V/L/I, the peptide may bind the FERM domain regardless of the combination of the two residues, although the binding affinity differs.

When cells are required to change their shape, this can be mediated by the plasmamembrane which is linked to the cytoskeleton by linker proteins such as the ERM proteins. If the connection between the cytoskeleton and adhesion molecules by linker proteins is necessary for the mediation of various morphological changes, it would not be unexpected to find that the specificity of the FERM binding motif is relatively low and reflected in a variety of binding molecules. Furthermore, a greater variety of as yet to be

identified adhesion molecules may be present that bind the FERM domain.

4.2 Comparison of the binding function among PTB-like domains

Our results support the notion that the peptide recognition mechanism of PTB-like subdomain C of ERM proteins differs from that of the canonical PTB domain and talin subdomain C. Key residues of the FERM domain involved in direct interactions with adhesion molecules are conserved in all ERM proteins (Figure 19A), and indicates that CD43 and PSGL-1 binding to other members of the ERM-protein family would essentially be the same as that reflected in the radixin FERM domain. Moreover, most of these residues are also conserved in the merlin FERM domain. However, residues in the FERM domain of talin or the canonical PTB domain that interact with adhesion molecules are poorly conserved (Figure 19AB). The PTB domain has been found in more than 200 protein molecules (Uhlik et al. 2005). The recognition motif of its binding partners is identical with rare exceptions, although the phosphorylation state of Tyr differs depending on the protein molecule. Talin, which comprises the FERM domain at the N-terminus just as with the ERM proteins (homology with radixin FERM domain is 24%), also recognizes the NPxY motif involved in binding to the integrin ß3 tail. This implies that the talin FERM domain possesses PTB domain function that differs from the ERM proteins. A recent report detailing the binding between the talin FERM domain and PIPKIγ indicated that the talin FERM domain recognizes the SPLH sequence, and although this sequence differs from NPxY the SPLH residues are located on the reverse turn, as is the case with the NPxY residues, and binds in a manner similar to the NPxY sequence (Figures 18B, C) (de Pereda et al. 2005). The number of PTB or PTB-like domains that include the FERM domain recognizing the NPxY motif is much greater than the number of ERM proteins type PTB-like domains. Although structural analyses

remain scant, other PTB-like domains that function as subdomain C of the ERM FERM domains does may emerge following future investigations. The FERM domain of merlin/schwanomin, the neurofibromatosis type 2 (NF2) tumor-suppressor gene products, can bind to CD44 and may possess properties similar to the ERM FERM domain (Sainio et al. 1997).

4.3 The relationship between adhesion molecules and ERM proteins in signaling.

A regulatory mechanism involving transition from a 'Dormant state' to an 'Active state' for ERM proteins has been suggested, and the mechanism involving targeting to the plasma membrane by adhesion molecules has been referred to in a previous report (Hamada et al. 2003). In this target mechanism, ERM proteins are engaged in the regulatory scheme under the regulation by small G-protein Rho and comprise a positive feedback loop through interaction with Rho-GDI (GDP dissociation inhibitor) (Takahashi et al. 1998). CD43 and PSGL-1 were shown to be excluded from the contact area related to immunological synapses formed at the interface between T-cells and antigen receptors (Montoya et al. 2002). Rho-GDI was also shown to be excluded from the immunological synapse interface and is localized with CD43 at opposite site of the immunological synapse (Allenspach et al. 2001). These findings seem to suggest that ERM proteins, Rho-GDI and CD43 interact through the FERM domain simultaneously. PSGL-1 was also shown to engage interaction with the aforementioned three molecules through the FERM domain. It has been reported that PSGL-1 bound to ERM proteins binds to non-receptor tyrosine kinase Syk through the same FERM domain, which facilitates activation of Syk and subsequent transmission of the signal downstream (Urzainqui et al. 2002).

Cells expressing adhesion molecules such as leukocytes can adopt a polarized

morphology from a globular shape through multiple phases of adhesion morphogenesis. The morphological changes of the plasmamembrane are based on the rapid rearrangement of the actin cytoskeleton mediated by cytoplasmic scaffold proteins such as ERM proteins. The physiological interaction between adhesion molecules and ERM proteins has been detailed in a number of reports and many adhesion molecules are thought to possess the FERM binding motif. Notwithstanding the plethora of reports detailing the aforementioned processes, the biological importance of the binding of adhesion molecules to ERM proteins, and whether ERM proteins control the function of adhesion molecules from the cytoplasmic site of contacts, remains poorly understood. CD43 and PSGL-1 belong to the sialomucin family, transmembrane type adhesion molecules, and do not possess the typical receptor domain since their extracellular domains are modified by glycosylation (Cyster et al. 1991; Maemura and Fukuda 1992). To date, no concrete model has been proffered that accounts for transmission of the extracellular signal. One report indicated that no change was observed in microvilli formation following expression of full-length CD43 or a chimeric CD43 molecule where the extracellular domain was replaced with the E-cadherin extracellular domain (Yonemura et al. 1993). Given that in this report we showed that the CD43 cytoplasmic tail exists in monomeric form and adopts an elongated shape without any clearly defined folded structure, it remains to be determined whether signal transduction is associated with conformational changes induced by binding to signaling molecules.

It is possible that ERM proteins send signals by forming a complex with various molecules at the juxtamembrane region as mentioned above. On the other hand, a distinct mechanism that involves signal transduction driven by the release of adhesion molecules from the plasmamembrane has also been presented. Many adhesion molecules possess extracellular domains that are segmented by matrix metalloproteinases (MMPs) belonging to type I transmembrane proteinases at the juxtamembrane, and is followed by

events where the cytoplasmic domains are segmented by PS (presenilin)-dependent γ-secretase (Itoh and Seiki 2006). The aforementioned processes have been suggested to operate with a number of molecules including CD44, syndecan and α_v integrin (Kajita et al. 2001; Deryugina et al. 2002; Endo et al. 2003). The release and secretion of PSGL-1 observed in human neutrophils and induced by PMA (phorbol ester) has also been observed in the case of the release of extracellular domains of many other protein molecules (Davenpeck et al. 2000). PSGL-1 is thought to have its extracellular domain segmented by either ß-secretase or BACE-1 (ß-site APP-cleaving enzyme) and, following this event, the cytoplasmic domain of PSGL-1 is thought to be separated into the cytoplasm by the action of γ-secretase (Lichtenthaler et al. 2003). Although CD43 is thought to be subjected to the same aforementioned processes, the involvement of MMP and secretase remains speculative. Although CD43 possesses a functional NLS (nuclear localization signal) sequence within the cytoplasmic domain, the cytoplasmic region was shown to be transferred into the nucleus and subsequently interact with ß catenin (Andersson et al. 2004; Andersson et al. 2005). The NLS sequence of CD43 is located at the juxtamembrane (280-194) region (Table 2) and overlaps the ERM binding motif. Aside from the NLS sequence, CD43 is phosphorylated by Ser/Thr kinase at the cytoplasmic domain (Wang et al. 2000) and is believed to represent the interaction site of the Src SH3 domain (Pedraza-Alva et al. 1998). The variety of roles played by CD43 in signal transduction remain to be full examined and future investigations, including examination of the relationship of ERM proteins, should provide useful insights into this complex signaling pathway.

Table 3 Binding affinities of CD43 and PSGL-1 for radixin FERM domain

		Sequence	*Kd*
CD43	272-395	GST- Full length	5.27 ± 0.15 μ M
CD43	272-291	Biotin- RQRQKRRTGALTLSGGGKRN	1.96 ± 0.19 μM
PSGL-1	331-362	Biotin- RLSRKTHMYPVRNYSPTEMVCISSLLPDGGEG	350 ± 93 n M
PSGL-1	331-348	Biotin- RLSRKTHMYPVRNYSPTE	201 ± 53 n M

K_d values were determined by BIACORE. The biotinylated peptides (PSGL-1; 18 residues and 32 residues and CD43 peptide; 20 residues) were chemically synthesized and the full length CD43 peptide was made as a recombinant GST fusion protein. The obtained K_d values with their standard deviations are shown. All measurements are conducted at 25°C, with HBP buffer (10mM HEPES-Na pH 7.4, 150mM NaCl, 1mM EDTA, 1mM DTT, 0.05% surfactant P20).

Table 4 Crystal data of the radixin FERM domain

Crystal data	FERM-CD43	FERM-PSGL-1
Crystal system	Tetragonal	Tetragonal
Spacegroup	$P4_322$	$P2_12_12_1$
Unit cell dimensions (Å)	$a = b = 68.72$, $c = 201.39$	$a = 80.74$, $b = 85.73$, $c = 117.75$
Z	8	4
V_M (Å^3/Da)	3.0	2.5
V_{solve} (%)	58.1	50.9

(left) the complex between the radixin FERM domain and the CD43 peptide
(right) the complex between the radixin FERM domain and the PSGL-1 peptide

Table 5 Crystallographic analysis of the FERM-CD43 complex and the FERM-PSGL-1 complex

Crystallographic analysis of the FERM-CD43 complex and the FERM-PSGL-1 complex		
	CD43	PSGL-1
Intensity data		
Resolution (Å)	2.9	2.8
Reflections		
Measured	90704	191709
Unique	11007	20429
Completeness (%) [a]	96.5 / 76.4	98.4 /92.3
R_{sym} [b] (%) [a]	12.1 / 37.7	7.1 /11.7
Mean I/σ [a]	7.7 / 1.7	9.2 / 3.7
Refinement		
Resolution range (Å)	50 – 2.9	50 – 2.8
Number of residues	331	668
Protein	316	626
Peptide	15	42
R_{cryst} factor / R_{free} factor	24.18 / 25.43	23.17 / 29.08
Mean B factor (Å^2)	74.1	43.7 (ABCDE)
Protein	72.5	42.6 (AB)
Peptide	108.6	60.6 (CD)
R.m.s. deviations [d]	0.010 Å, 1.827 °	0.008 Å, 1.391 °

[a] Each pair of values are for overall/outer shell. The resolution ranges of their outer shells are 2.9-2.8 Å (PSGL-1/FERM), 3.0-2.9 Å (CD43/FERM) .

[b] $R_{sym} = \Sigma | I - \langle I \rangle | / \Sigma I$; calculated for all data.

[c] R_{cryst} and $R_{free} = \Sigma | | F_o | - | F_c | | / \Sigma | F_o |$, where the free reflections (10% of the total used) were held aside for R_{free} throughout refinement.

[d] The two values are for bond lengths and bond angles.

Table 6 Solutions of rotation function and translation function

(radixin FERM/CD43 complex)

θ	φ	χ	X	Y	Z	*R*-fac	*Corr*
45.53	**0.00**	**44.87**	**0.098**	**0.698**	**0.094**	**0.372**	**0.750**
41.00	72.13	22.44	0.309	0.756	0.158	0.590	0.331
80.92	62.69	7.63	0.089	0.609	0.173	0.582	0.336

(radixin FERM/PSGL-1 complex)

Mol 1	θ	φ	χ	X	Y	Z	*R-fac*	*Corr*
	149.55	**76.47**	**212.87**	**0.412**	**0.181**	**0.432**	**0.656**	**0.242**
	86.69	90.00	260.16	0.437	0.118	0.239	0.700	0.131
	49.16	30.38	338.08	0.591	0.066	0.303	0.688	0.146

Mol2	θ	φ	χ	X	Y	Z	*R-fac*	*Corr*
	149.55	**76.47**	**212.87**	**0.321**	**0.680**	**0.432**	**0.522**	**0.567**
	49.16	30.38	338.08	0.095	0.823	0.574	0.669	0.203
	54.58	44.60	90.03	0.917	0.424	0.928	0.672	0.198

Solutions of rotation and translation functions with the correlation coefficient (*Corr*), and *R*-factor (*R-fac*)
Three solutions are gave in order of correlation coefficient values with the most probable solution in bold. (θφχ) are the polar angles and (XYZ) are fractional coordinates.

(The FERM-CD43 complex)
Reflections between 48-3 Å were used in the calculations. The radius of integration is 38 Å. The space group $P4_322$ gave the highest *C* and the lowest *R*.

(The FERM-PSGL-1 complex)
Reflections between 48-3 Å were used in the calculations with the radius of integration of 43 Å. The space group $P2_12_12_1$ gave the highest *C* and the lowest *R*. This crystal contains two complexes per asymmetric unit.

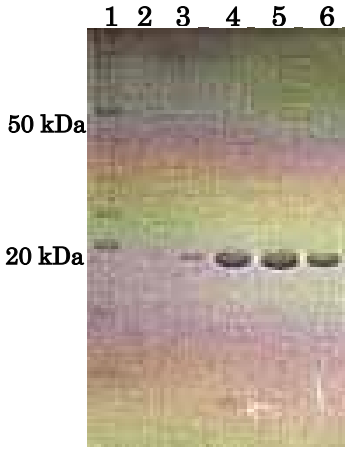

Figure 5　SDS-PAGE of CD43 cytoplasmic domain

Lane 1: Molecular weight markers (10 kDa ladder).
Lanes 2-6:　Purified CD43 cytoplasmic domain.

A

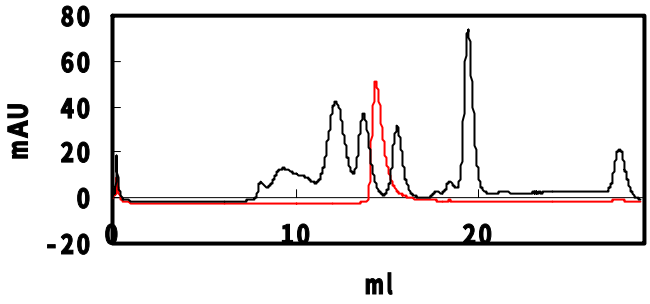
80
60
40
20
0
-20
mAU
0
10
20
ml

B

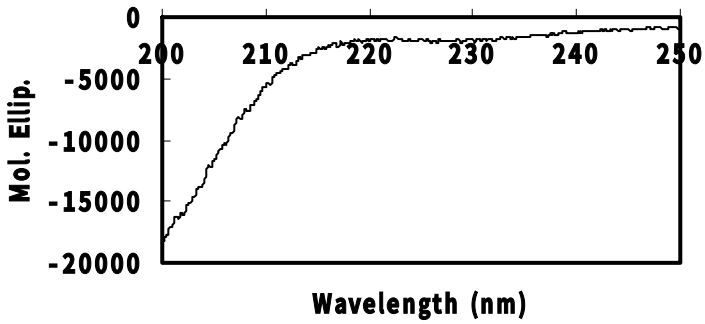
0
-5000
-10000
-15000
-20000
Mol. Ellip.
200
210
220
230
240
250
Wavelength (nm)

C

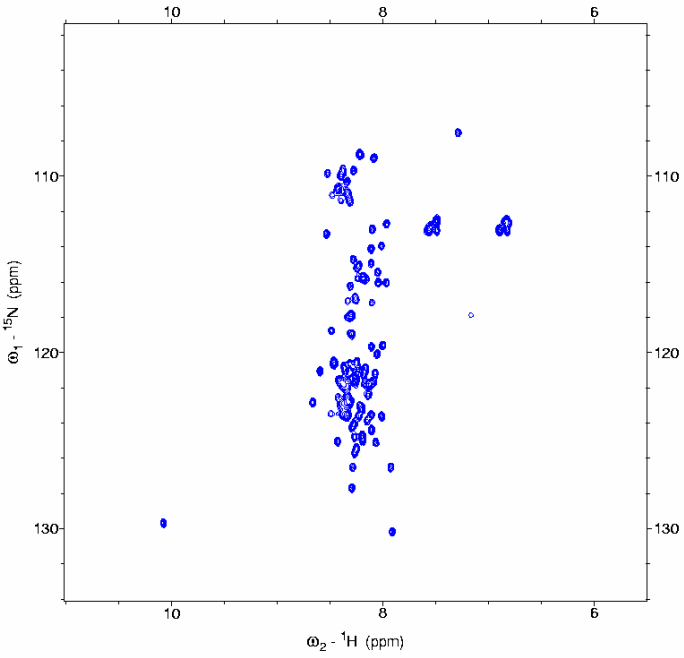
10
8
6
110
120
130
ω1 - 15N (ppm)
ω2 - 1H (ppm)

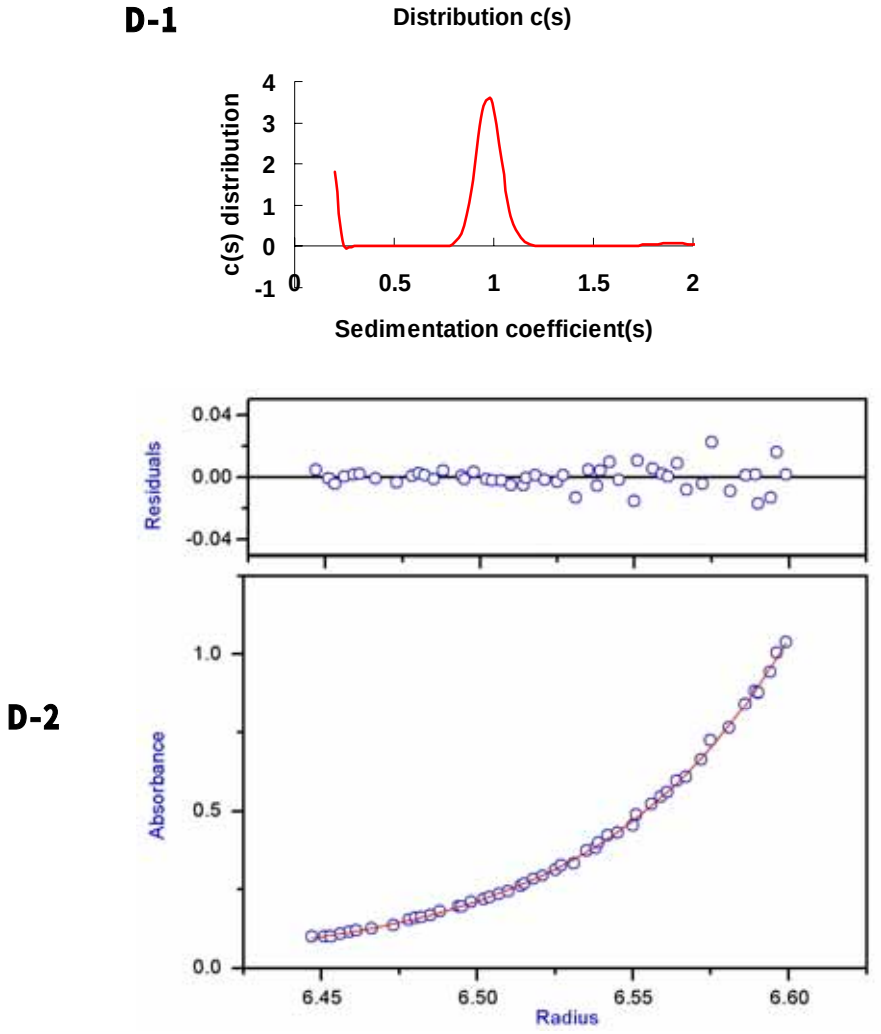

Figure 6 NMR and hydrodynamic studies of the CD43 cytoplasmic tail in solution

(A) The analytical gel filtration chromatogram of the CD43 cytoplasmic tail
The chromatogram of a standard protein sample is shown in black and the CD43 cytoplasmic tail is shown in red. The number at each peak is molecular weight (kDa). The MW of CD43 (32kDa) was calculated from standard protein chromatogram. Standard protein: bovine γ-globulin (*158*), chicken ovalbumin (*44*), equine myoglobin (*17*), and vitamin B-12 (*1.4*) (Bio-Rad).
(B)A far-UV CD spectrum of the CD43 cytoplasmic tail
(C) The NMR spectrum of the ^{15}N label CD43 cytoplasmic tail peptide
Measurements were conducted under the condition as follows, buffer: 20mM MES pH6.8, 100mM NaCl, 1mM DTT, 1mM EDTA, CD43: 250μM
(D) The results of analytical ultra centrifugation of the CD43 cytoplasmic tail
(D-1) Sedimentation velocity analysis for the CD43 cytoplasmic tail
The distribution of sedimentation coefficient is shown. The single peak is found at 1S. This distribution indicates a monomer molecule.
(D-2) Sedimentation equilibrium analysis for the CD43 cytoplasmic tail
The residuals of the fit are shown. Best fit curves for the CD43 cytoplasmic tail at a rotor speed of 39,000 rpm using absorbance optics. The concentration is 1.4 mg/ml. The fit assumed a single species and gave molecular masses of 12,200 Da.

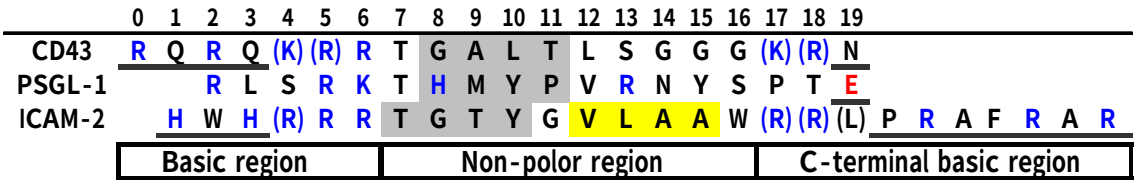

Figure 7 The sequences used for structural work

Based on the mouse proteins, 20-residue (CD43) and 18-residue (PSGL-1) peptides were synthesized for crystallization. Basic residues are in blue and acidic residues in red. These peptides have two basic regions and a non-polar region between them. The residues shown underlined were not defined on the current map. The short ß-strand (residues 7-10 or 8-11) and 3_{10} helix (resides 12-15) are highlighted gray and yellow respectively. The residues in parentheses are alanine in the current models. The number on the top column is the residue number.

A

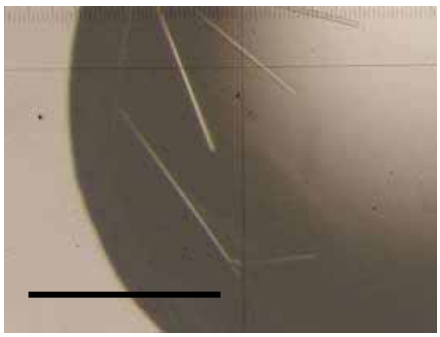

(A) radixin FERM / CD43	
Protein : Peptide	1 : 5 molar ratio
Reservoir	10% PEG4K, 10% 2-propanol, 100 mM Na-Citrate (pH5.6)
Temp	4 ˚C

B

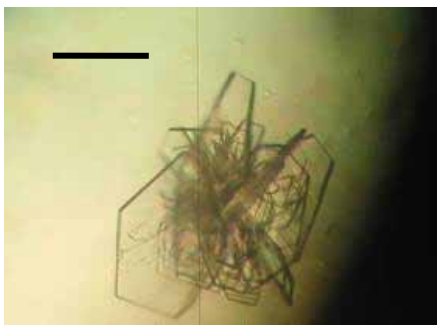

(B) radixin FERM / PSGL-1	
Protein : Peptide	1 : 10 molar ratio
Reservoir	8% PEG8K, 100 mM Tris-HCl (pH8.2)
Temp	4 ˚C

Figure 8 Crystal of the radixin FERM domain and crystallization condition

(A) The scale bar indicates 0.1 mm.
(B) The scale bar indicates 0.2 mm.

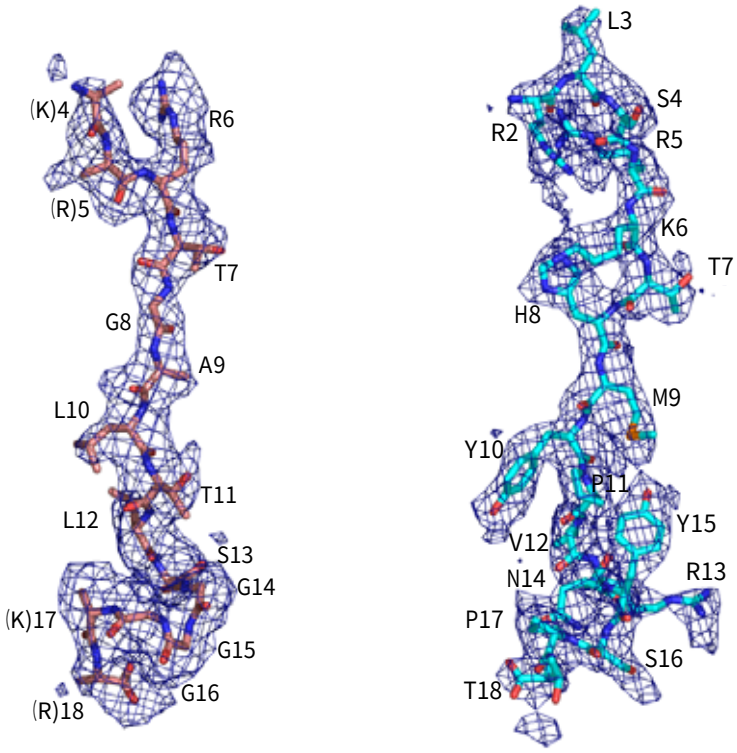

Figure 9 The electron density for the FERM-bound peptides

The CD43 (left) and PSGL-1 (right) peptide models in a 2Fo-Fc electron density map countered at the 1σ level. The amino acid residues are indicated with labels of one-letter codes. Labels in parentheses indicate the terminal residues whose side chains were not defined in the map.

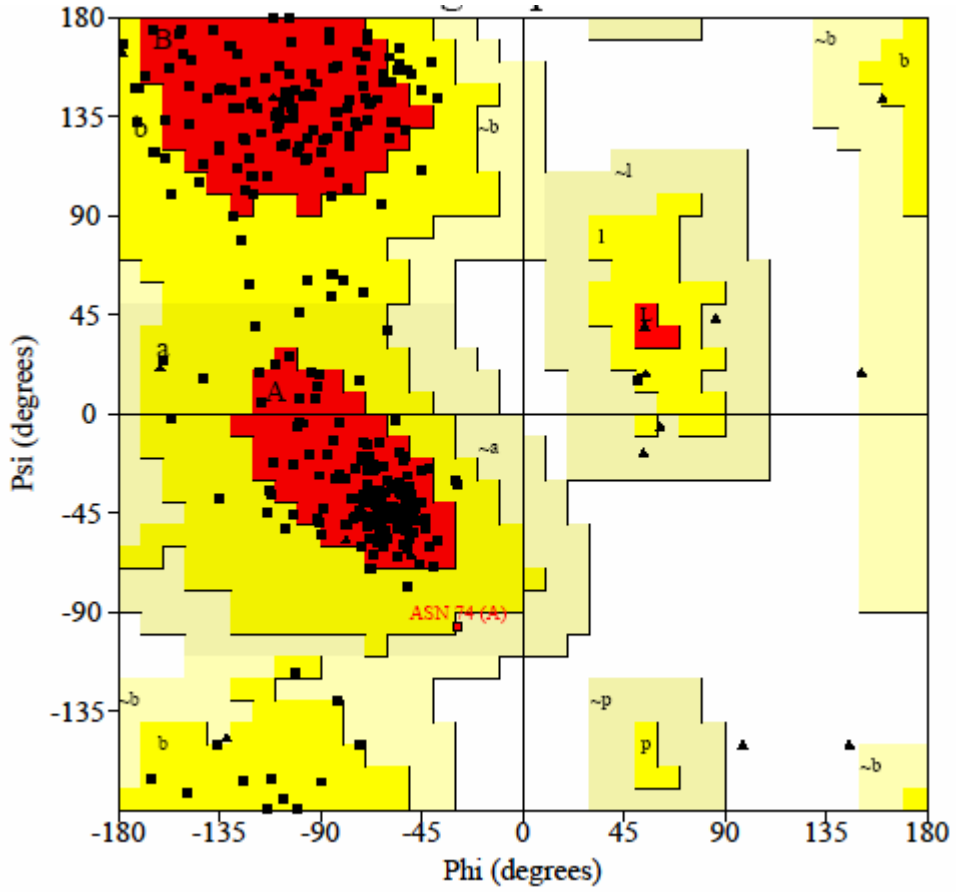

Plot statistics

Residues in most favoured regions [A,B,L]	236	80.0%
Residues in additional allowed regions [a,b,l,p]	58	19.7%
Residues in generously allowed regions [~a,~b,~l,~p]	1	0.3%
Residues in disallowed regions	0	0.0%

Figure 10.1 Ramachandran plot of the FERM-CD43 complex

Analysis of main chain angles was performed using *PROCHECK* software. Φ angle around N-C_α bond is indicated on the horizontal axis and ψ angle around C_α-C bond is indicated on the vertical axis. Glycine residues are shown as triangles, all residues except for glycine residues are shown as squares. Most favored, additional allowed, generously allowed and disallowed regions are shaded in red, yellow, light yellow and white, respectively. The labels of A and a indicate the regions for α-helix, B and b for β-strand, and L and l for α_L-helix. No residues are found in the disallowed region. There are 81.7% residues in most favored regions.

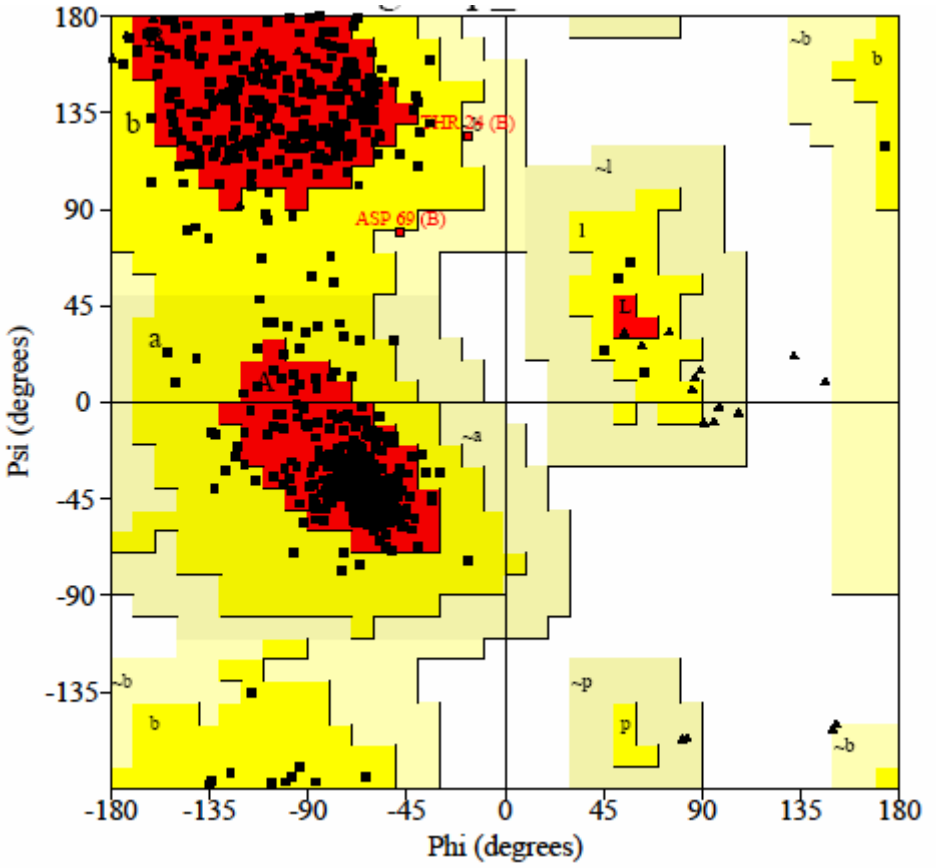

Plot statistics

Residues in most favoured regions [A,B,C]	523	87.6%
Residues in additional allowed regions [a,b,l,p]	72	12.1%
Residues in generously allowed regions [~a,~b,~l,~p]	2	3%
Residues in disallowed regions	0	0.0%

Figure 10.2 Ramachandran plot of the FERM-PSGL-1 complex

No residues are found in the disallowed region. There are 87.6% residues in most favored regions.

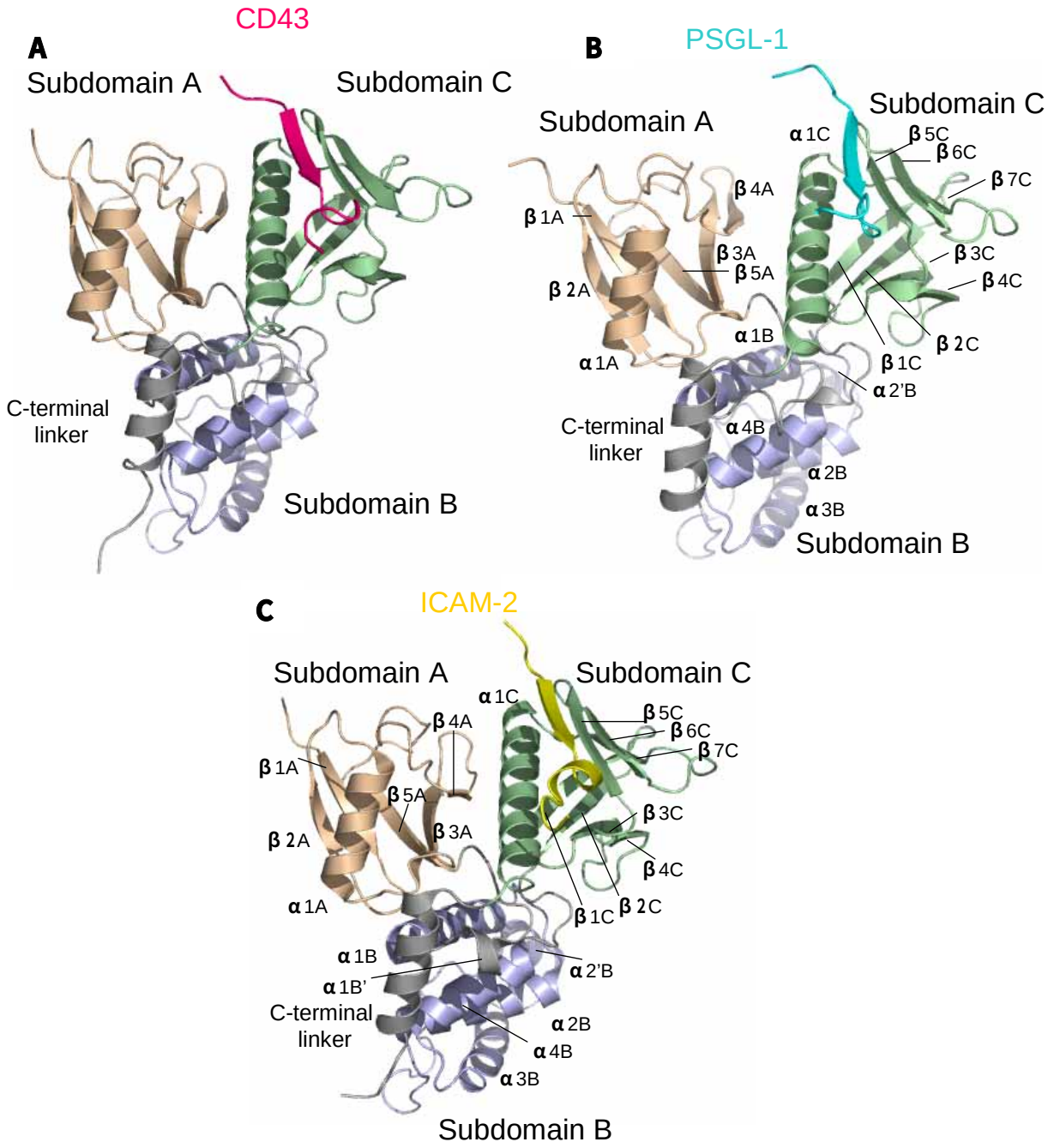

Figure 11 Overall structure of the radixin FERM domain bound to the adhesion molecule peptides

Views of the radixin FERM domain bound to adhesion molecule peptides by ribbon representations. The CD43 peptide is shown in pink, the PSGL-1 peptide in blue and the ICAM-2 peptide is shown in yellow. The radixin FERM domain consists of subdomain A (wheat), B (light blue) and C (pale green). The linkers A-B (residues 83-95), B-C (residues 196-203) and the C-terminal linker are colored in gray. The binding cite is same as ICAM-2 peptide.

(A) The FERM-CD43 complex

(B) The FERM- PSGL-1 complex

(C) The FERM-ICAM-2 complex

Table 7 Structural comparison among three radixin FERM domains

CD43	FERM Free Form	FERM IP_3 Form	FERM ICAM-2 Form
FERM domain	1.653	1.601	0.637
Subdomain AB	1.329	1.304	0.700
Subdomain BC	0.951	0.937	0.492
Subdomain A	0.526	0.525	0.637
Subdoamin B	0.811	0.831	0.470
Subdomain C	0.985	0.927	0.379

PSGL-1	FERM Free Form	FERM IP_3 Form	FERM ICAM-2 Form
FERM domain	0.771	0.773	1.279
Subdomain AB	0.707	0.709	0.882
Subdomain BC	0.871	0.857	0.767
Subdomain A	0.503	0.501	0.572
Subdoamin B	0.792	0.809	0.415
Subdomain C	0.835	0.805	0.483

(Upper table) The FERM domain bound to the CD43 peptide is compared to the free, IP3-bound, ICAM-2-bound forms, respectively.
(Lower table) The same comparison with the FERM domain bound to the PSGL-1 peptide. By using LSQKAB (Collaborative Computational Project No. 4., 1994), obtained average r.m.s. deviations (Å) are listed. Superposition is conducted on overall structure, subomain AB, BC, subomain A, B, and C in each.

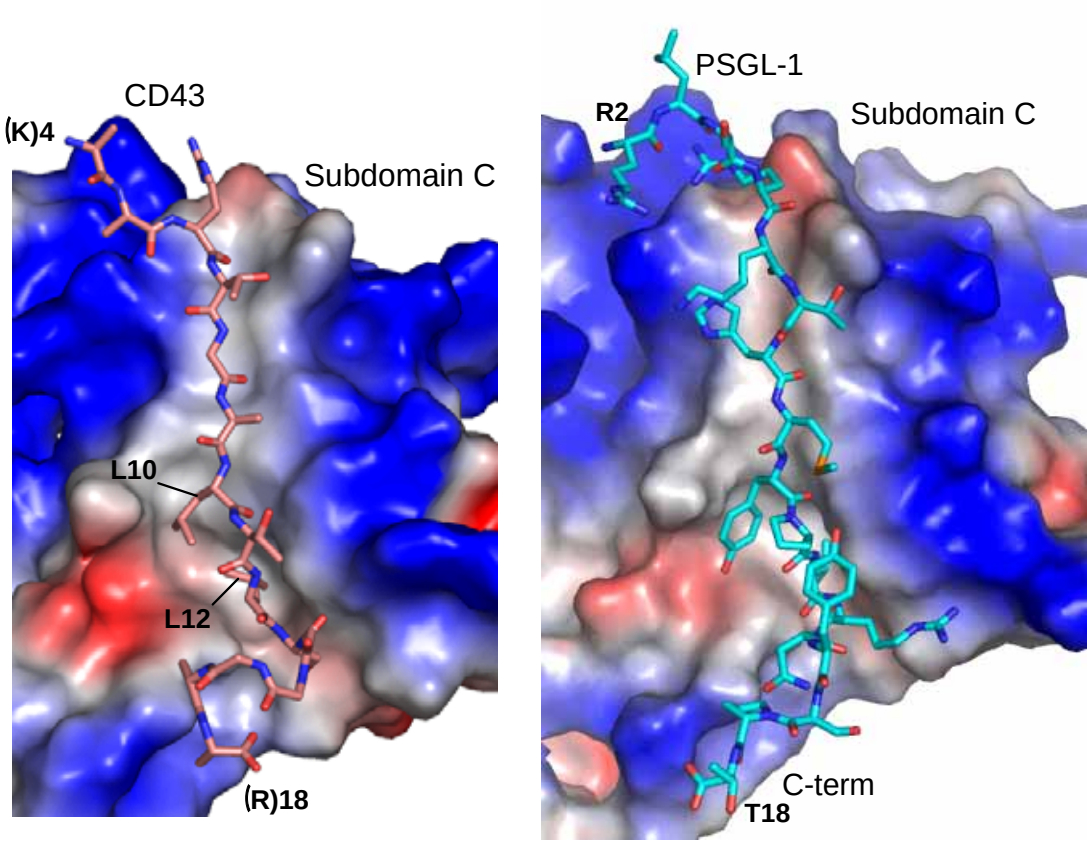

Figure 12 Surface electrostatic potentials of the radixin FERM domain

Positive (blue) and negative (red) potentials are mapped on the van der Waals surfaces. The CD43 (pink in right) and PSGL-1 (blue in left) peptides found in the complex crystals are shown in stick models. These adhesion molecule peptides bind along the hydrophobic groove of FERM subdomain C.

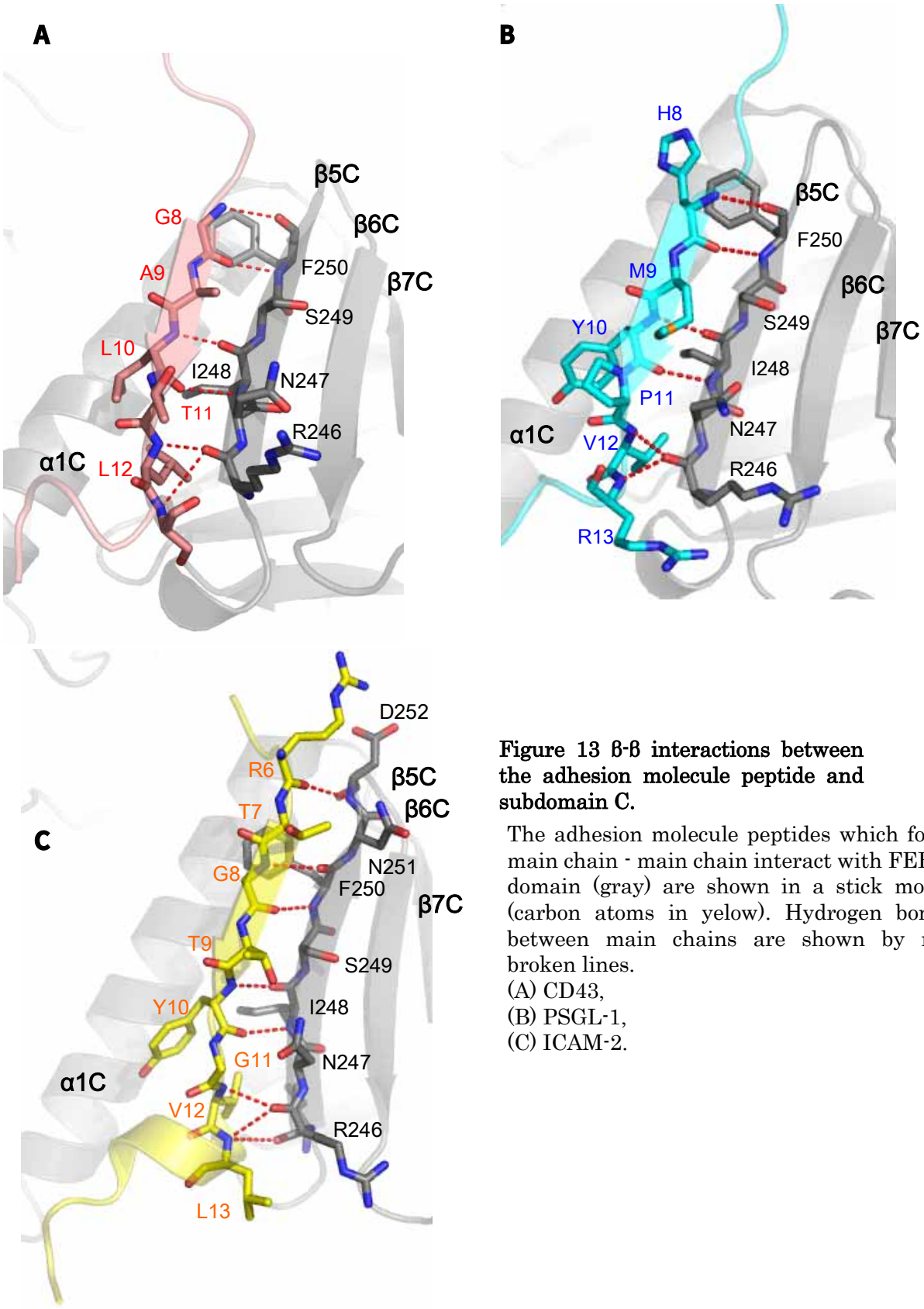

Figure 13 β-β interactions between the adhesion molecule peptide and subdomain C.

The adhesion molecule peptides which form main chain - main chain interact with FERM domain (gray) are shown in a stick model (carbon atoms in yelow). Hydrogen bonds between main chains are shown by red broken lines.
(A) CD43,
(B) PSGL-1,
(C) ICAM-2.

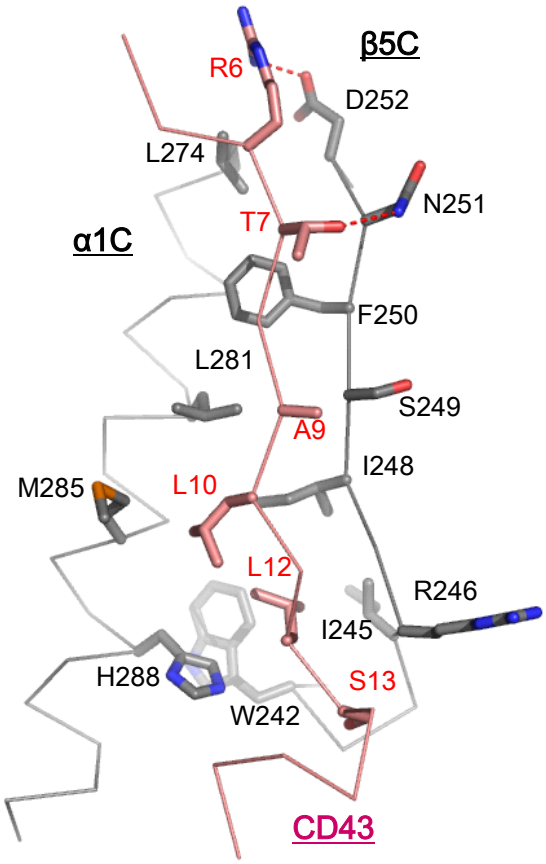
β5C
R6
D252
L274
N251
T7
α1C
F250
L281
S249
A9
I248
M285
L10
L12
R246
I245
H288
S13
W242
CD43

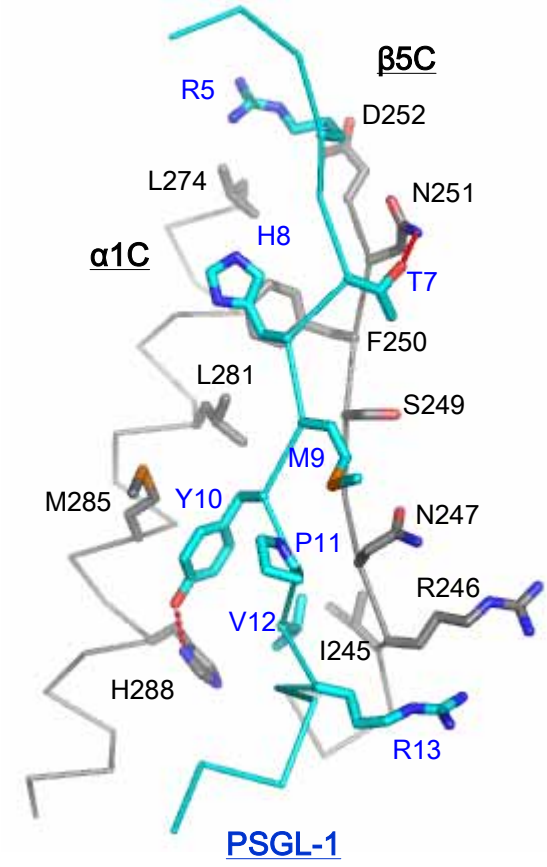
β5C
R5
D252
L274
N251
H8
α1C
T7
F250
L281
S249
M9
M285
Y10
N247
P11
R246
V12
I245
H288
R13
PSGL-1

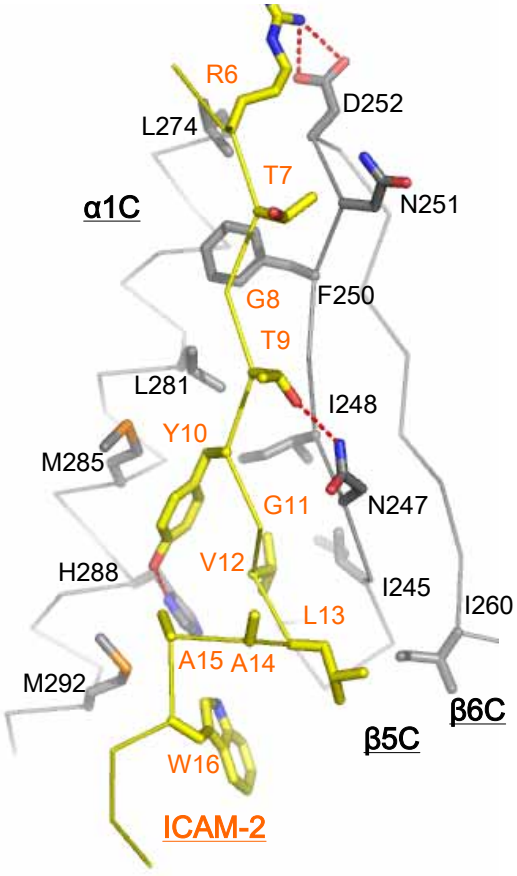
R6
D252
L274
T7
α1C
N251
G8
F250
T9
L281
I248
Y10
M285
G11
N247
V12
H288
I245
I260
L13
A15
A14
M292
β6C
β5C
W16
ICAM-2

Figure 14 The side chain-side chain interactions found in the FERM-peptide complex

The side chain which are shown in stick model are involved the interaction. The CD43 peptide (pink), PSGL-1 peptide (blue), ICAM-2 peptide (yellow) and helix α1C and strand β5C of subdomain C (gray). Hydrogen bonds between side chains are shown by red broken lines.

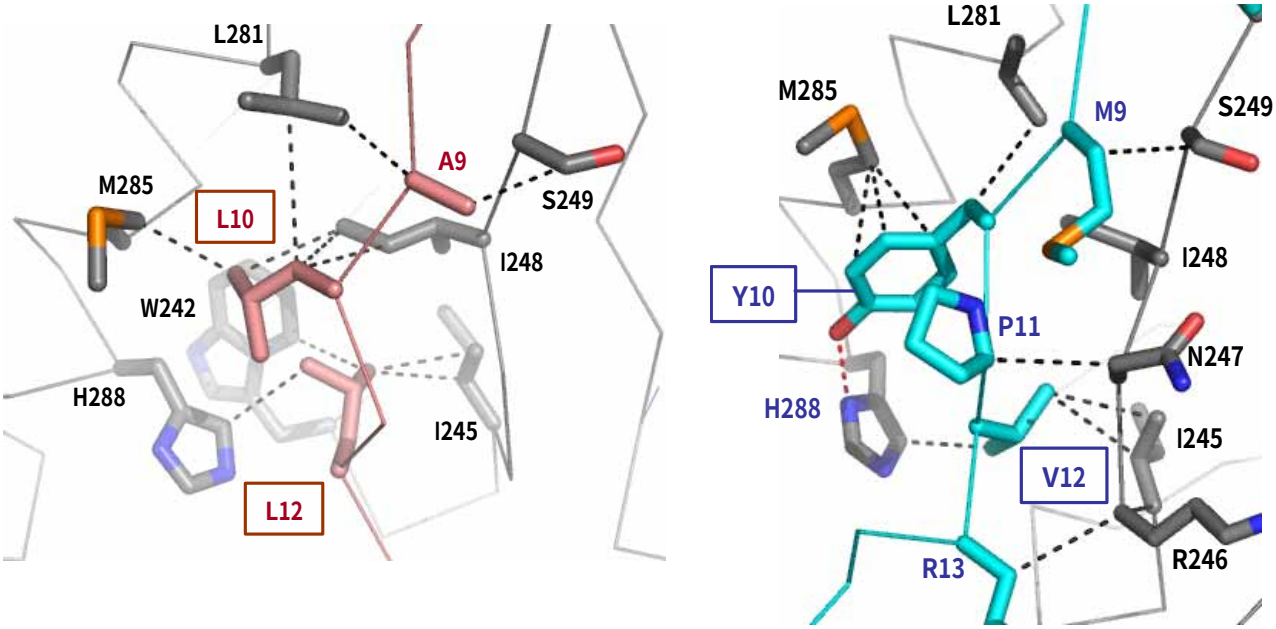

Figure 15 Close-up views of side chain-side chain interactions around L10-L12 (CD43) and Y10-V12 (PSGL-1)

The interactions among side chains around the residues (10-12) are shown. The side chains which are shown in stick models are involved the interactions. The CD43 peptide (pink) and the PSGL-1 peptide (blue) bound to the hydrophobic pocket of subdomain C (gray) are highlighted. Hydrogen bonds between side chains are shown by red broken lines and hydrophobic interactions are shown by black broken lines.

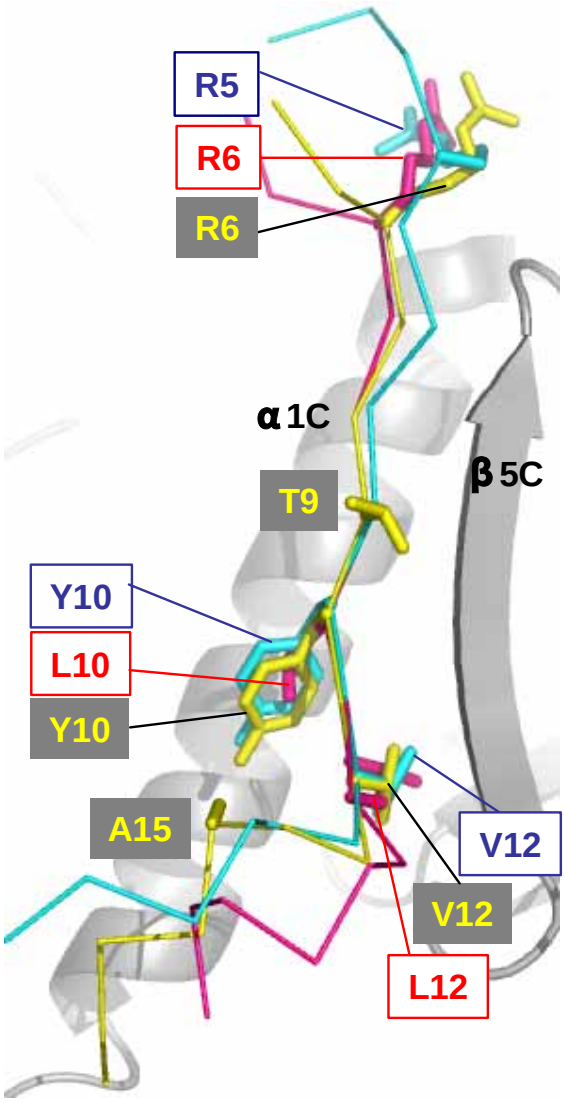

Figure 16 The comparison among the interaction cite of adhesion molecules

The FERM-CD43 and FERM-PSGL-1 complex structures are superimposed on the FERM-ICAM-2 complex. Color codes are gray for the ICAM-2-bound FERM domain, yellow for ICAM-2, pink for CD43 and blue for PSGL-1. The side chains which are shown in stick models are the key residues for FERM binding.

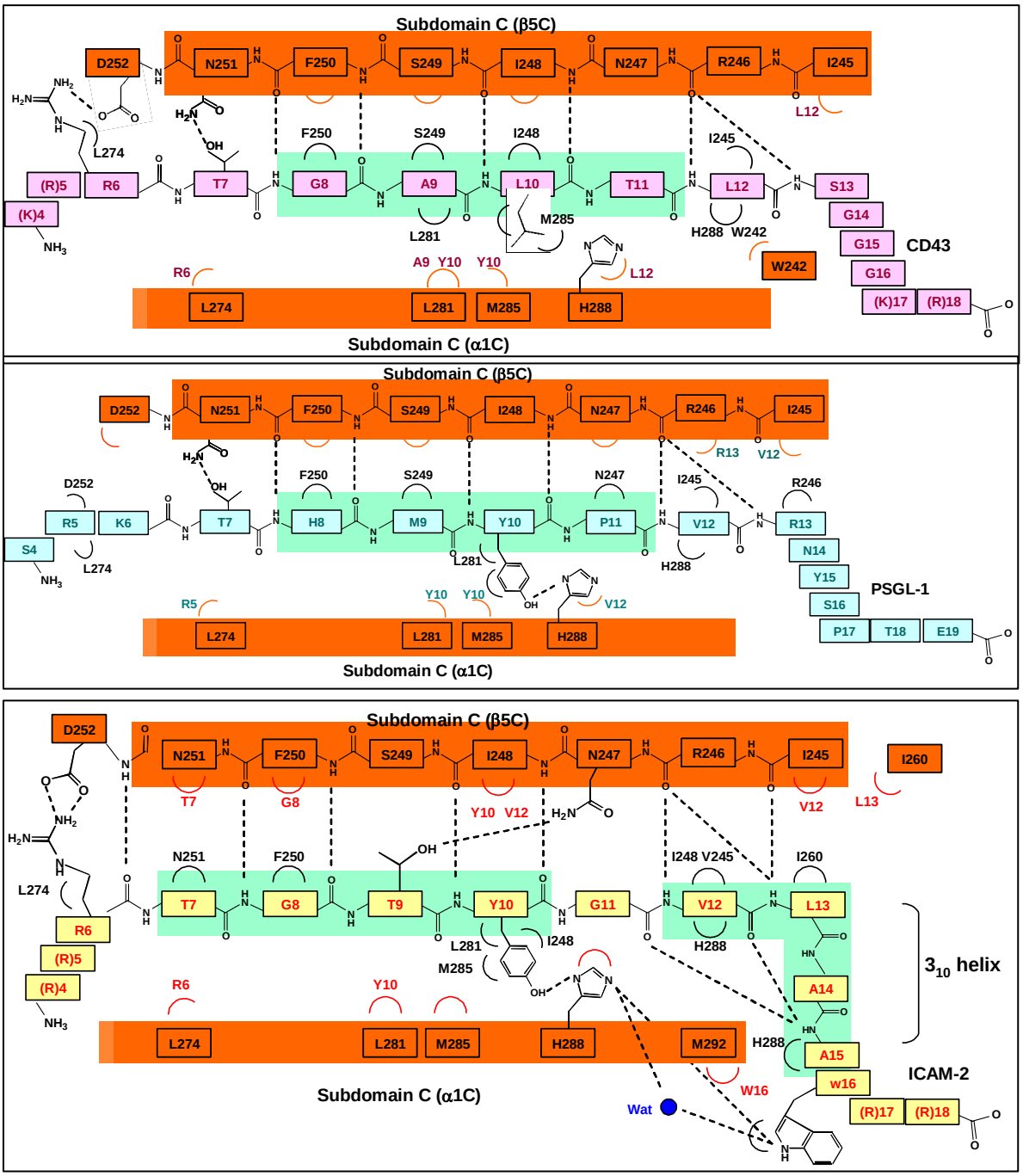

Figure 17 Schematic representation of the interactions between the adhesion molecule peptide and the radixin FERM subdomain C

Hydrogen bonds are shown by broken lines. Semicircle lines show hydrophobic interactions. Upper: CD43, middle: PSGL-1, lower: ICAM-2.

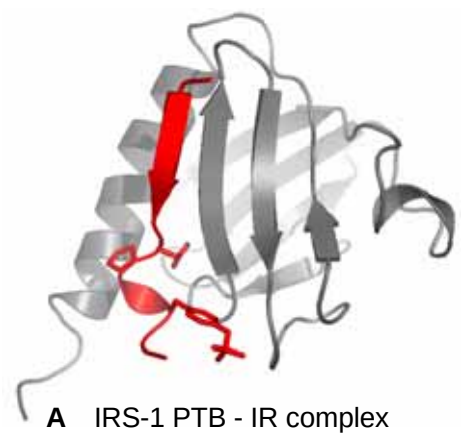

A IRS-1 PTB - IR complex

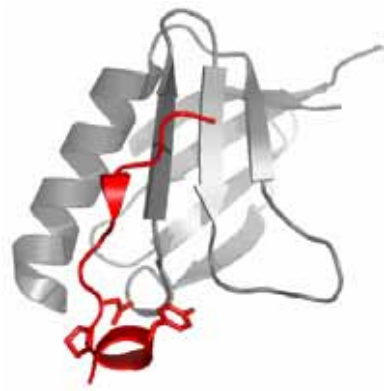

B Talin FERM - Integrin β3 complex

C Talin FERM - PIPK Ⅰγ complex

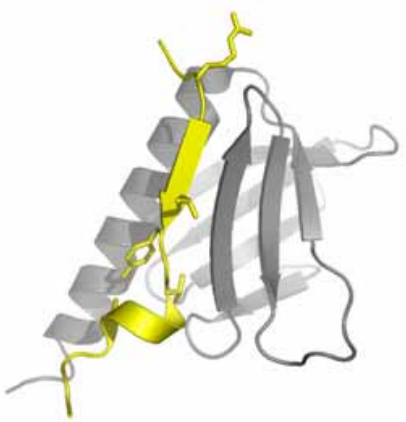

D Radixin FERM - ICAM-2 complex

E Radixin FERM – CD43 complex

F Radixin FERM – PSGL-1 complex

Figure 18 Comparison of peptide structures bound to the FERM subdomain C and the canonical PTB domain

Ribbon representations in gray are FERM subdomain C or PTB domain. The side chains of the FERM-binding motif are shown in stick models. PDB accession number: 1IRS(A), 1MK7(B), 1y19 (C), 1J19(D)

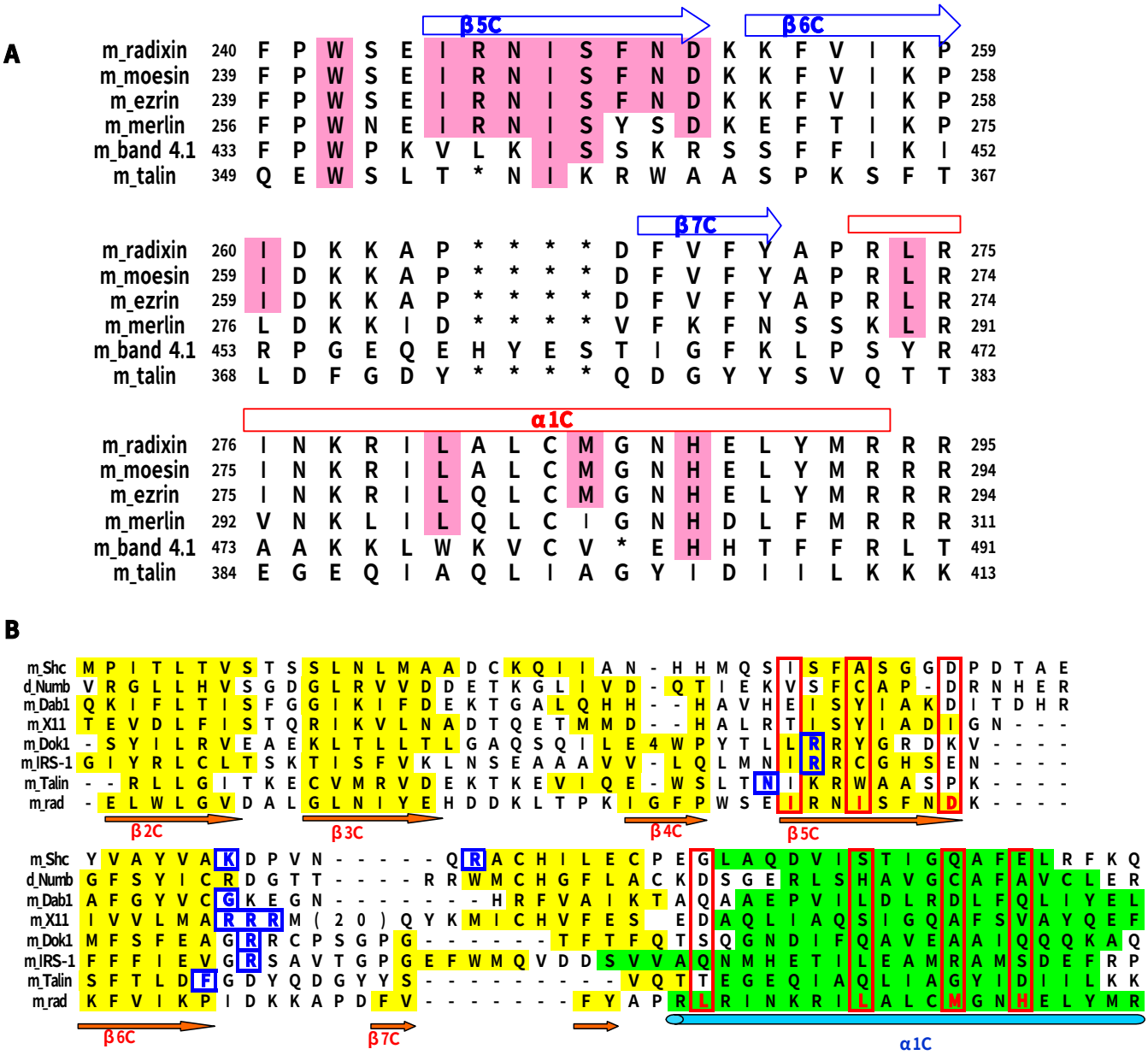

Figure 19 Sequence alignments of subdomain C from related FERM domains and PTB domains

(A) The FERM subdomain C of mouse radixin, ezrin, moesin, human band 4.1 (hP 4.1) and talin (mTalin) are aligned with the secondary structure elements of the radixin FERM subdomain C at the top: α -helix (rectangle) and β -strands (arrow). The residues highlighted in pink participate in nonpolar and polar interactions with the radixin FERM domain and the PSGL-1 or CD43 peptide.
(B) The FERM subdomain C of mouse radixin, several PTB domains and talin sabdomain C are aligned with the secondary structure elements of the radixin FERM subdomain C. The residues highlighted in yellow show ß sheet and in green show α helix. Residues in the radixin FERM subdomain C that interact with the PSGL-1 and CD43 peptide are colored in red. Residues in PTB domains that interact with the tyrosin or phosphotyrosine residue are boxed in blue.

5 References

1994. The CCP4 suite: programs for protein crystallography. *Acta Crystallogr D Biol Crystallogr* **50:** 760-763.

Allenspach, E.J., Cullinan, P., Tong, J., Tang, Q., Tesciuba, A.G., Cannon, J.L., Takahashi, S.M., Morgan, R., Burkhardt, J.K., and Sperling, A.I. 2001. ERM-dependent movement of CD43 defines a novel protein complex distal to the immunological synapse. *Immunity* **15:** 739-750.

Andersson, C.X., Fernandez-Rodriguez, J., Laos, S., Baeckstrom, D., Haass, C., and Hansson, G.C. 2005. Shedding and gamma-secretase-mediated intramembrane proteolysis of the mucin-type molecule CD43. *Biochem J* **387:** 377-384.

Andersson, C.X., Fernandez-Rodriguez, J., Laos, S., Sikut, R., Sikut, A., Baeckstrom, D., and Hansson, G.C. 2004. CD43 has a functional NLS, interacts with beta-catenin, and affects gene expression. *Biochem Biophys Res Commun* **316:** 12-17.

Andreoli, C., Martin, M., Le Borgne, R., Reggio, H., and Mangeat, P. 1994. Ezrin has properties to self-associate at the plasma membrane. *J Cell Sci* **107 (Pt 9):** 2509-2521.

Balla, T. 2005. Inositol-lipid binding motifs: signal integrators through protein-lipid and protein-protein interactions. *J Cell Sci* **118:** 2093-2104.

Barreiro, O., Yanez-Mo, M., Serrador, J.M., Montoya, M.C., Vicente-Manzanares, M., Tejedor, R., Furthmayr, H., and Sanchez-Madrid, F. 2002. Dynamic interaction of VCAM-1 and ICAM-1 with moesin and ezrin in a novel endothelial docking structure for adherent leukocytes. *J Cell Biol* **157:** 1233-1245.

Bretscher, A., Edwards, K., and Fehon, R.G. 2002. ERM proteins and merlin: integrators at the cell cortex. *Nat Rev Mol Cell Biol* **3:** 586-599.

Brunger, A.T., Adams, P.D., Clore, G.M., DeLano, W.L., Gros, P., Grosse-Kunstleve, R.W., Jiang, J.S., Kuszewski, J., Nilges, M., Pannu, N.S., et al. 1998. Crystallography & NMR system: A new software suite for macromolecular structure determination. *Acta*

Crystallogr D Biol Crystallogr **54:** 905-921.

Cheng, L., Itoh, K., and Lemmon, V. 2005. L1-mediated branching is regulated by two ezrin-radixin-moesin (ERM)-binding sites, the RSLE region and a novel juxtamembrane ERM-binding region. *J Neurosci* **25:** 395-403.

Chishti, A.H., Kim, A.C., Marfatia, S.M., Lutchman, M., Hanspal, M., Jindal, H., Liu, S.C., Low, P.S., Rouleau, G.A., Mohandas, N., et al. 1998. The FERM domain: a unique module involved in the linkage of cytoplasmic proteins to the membrane. *Trends Biochem Sci* **23:** 281-282.

Cyster, J.G., Shotton, D.M., and Williams, A.F. 1991. The dimensions of the T lymphocyte glycoprotein leukosialin and identification of linear protein epitopes that can be modified by glycosylation. *Embo J* **10:** 893-902.

Davenpeck, K.L., Brummet, M.E., Hudson, S.A., Mayer, R.J., and Bochner, B.S. 2000. Activation of human leukocytes reduces surface P-selectin glycoprotein ligand-1 (PSGL-1, CD162) and adhesion to P-selectin in vitro. *J Immunol* **165:** 2764-2772.

de Pereda, J.M., Wegener, K.L., Santelli, E., Bate, N., Ginsberg, M.H., Critchley, D.R., Campbell, I.D., and Liddington, R.C. 2005. Structural basis for phosphatidylinositol phosphate kinase type Igamma binding to talin at focal adhesions. *J Biol Chem* **280:** 8381-8386.

Deryugina, E.I., Ratnikov, B.I., Postnova, T.I., Rozanov, D.V., and Strongin, A.Y. 2002. Processing of integrin alpha(v) subunit by membrane type 1 matrix metalloproteinase stimulates migration of breast carcinoma cells on vitronectin and enhances tyrosine phosphorylation of focal adhesion kinase. *J Biol Chem* **277:** 9749-9756.

Dickson, T.C., Mintz, C.D., Benson, D.L., and Salton, S.R. 2002. Functional binding interaction identified between the axonal CAM L1 and members of the ERM family. *J Cell Biol* **157:** 1105-1112.

Eck, M.J., Dhe-Paganon, S., Trub, T., Nolte, R.T., and Shoelson, S.E. 1996. Structure of the

IRS-1 PTB domain bound to the juxtamembrane region of the insulin receptor. *Cell* **85:** 695-705.

Edwards, S.D., and Keep, N.H. 2001. The 2.7 A crystal structure of the activated FERM domain of moesin: an analysis of structural changes on activation. *Biochemistry* **40:** 7061-7068.

Endo, K., Takino, T., Miyamori, H., Kinsen, H., Yoshizaki, T., Furukawa, M., and Sato, H. 2003. Cleavage of syndecan-1 by membrane type matrix metalloproteinase-1 stimulates cell migration. *J Biol Chem* **278:** 40764-40770.

Fievet, B.T., Gautreau, A., Roy, C., Del Maestro, L., Mangeat, P., Louvard, D., and Arpin, M. 2004. Phosphoinositide binding and phosphorylation act sequentially in the activation mechanism of ezrin. *J Cell Biol* **164:** 653-659.

Fukata, Y., Kimura, K., Oshiro, N., Saya, H., Matsuura, Y., and Kaibuchi, K. 1998. Association of the myosin-binding subunit of myosin phosphatase and moesin: dual regulation of moesin phosphorylation by Rho-associated kinase and myosin phosphatase. *J Cell Biol* **141:** 409-418.

Garcia-Alvarez, B., de Pereda, J.M., Calderwood, D.A., Ulmer, T.S., Critchley, D., Campbell, I.D., Ginsberg, M.H., and Liddington, R.C. 2003. Structural determinants of integrin recognition by talin. *Mol Cell* **11:** 49-58.

Gary, R., and Bretscher, A. 1995. Ezrin self-association involves binding of an N-terminal domain to a normally masked C-terminal domain that includes the F-actin binding site. *Mol Biol Cell* **6:** 1061-1075.

Granes, F., Berndt, C., Roy, C., Mangeat, P., Reina, M., and Vilaro, S. 2003. Identification of a novel Ezrin-binding site in syndecan-2 cytoplasmic domain. *FEBS Lett* **547:** 212-216.

Haas, M.A., Vickers, J.C., and Dickson, T.C. 2004. Binding partners L1 cell adhesion molecule and the ezrin-radixin-moesin (ERM) proteins are involved in development and the regenerative response to injury of hippocampal and cortical neurons. *Eur J Neurosci*

20: 1436-1444.

Hamada, K., Shimizu, T., Matsui, T., Tsukita, S., and Hakoshima, T. 2000. Structural basis of the membrane-targeting and unmasking mechanisms of the radixin FERM domain. *Embo J* **19:** 4449-4462.

Hamada, K., Shimizu, T., Matsui, T., Tsukita, S., Tsukita, S., and Hakoshima, T. 2001. Crystallographic characterization of the radixin FERM domain bound to the cytoplasmic tail of the adhesion protein ICAM-2. *Acta Crystallogr D Biol Crystallogr* **57:** 891-892.

Hamada, K., Shimizu, T., Yonemura, S., Tsukita, S., Tsukita, S., and Hakoshima, T. 2003. Structural basis of adhesion-molecule recognition by ERM proteins revealed by the crystal structure of the radixin-ICAM-2 complex. *Embo J* **22:** 502-514.

Heiska, L., Alfthan, K., Gronholm, M., Vilja, P., Vaheri, A., and Carpen, O. 1998. Association of ezrin with intercellular adhesion molecule-1 and -2 (ICAM-1 and ICAM-2). Regulation by phosphatidylinositol 4, 5-bisphosphate. *J Biol Chem* **273:** 21893-21900.

Helander, T.S., Carpen, O., Turunen, O., Kovanen, P.E., Vaheri, A., and Timonen, T. 1996. ICAM-2 redistributed by ezrin as a target for killer cells. *Nature* **382:** 265-268.

Hirao, M., Sato, N., Kondo, T., Yonemura, S., Monden, M., Sasaki, T., Takai, Y., Tsukita, S., and Tsukita, S. 1996. Regulation mechanism of ERM (ezrin/radixin/moesin) protein/plasma membrane association: possible involvement of phosphatidylinositol turnover and Rho-dependent signaling pathway. *J Cell Biol* **135:** 37-51.

Itoh, Y., and Seiki, M. 2006. MT1-MMP: a potent modifier of pericellular microenvironment. *J Cell Physiol* **206:** 1-8.

Ivetic, A., Deka, J., Ridley, A., and Ager, A. 2002. The cytoplasmic tail of L-selectin interacts with members of the Ezrin-Radixin-Moesin (ERM) family of proteins: cell activation-dependent binding of Moesin but not Ezrin. *J Biol Chem* **277:** 2321-2329.

Iwase, A., Shen, R., Navarro, D., and Nanus, D.M. 2004. Direct binding of neutral

endopeptidase 24.11 to ezrin/radixin/moesin (ERM) proteins competes with the interaction of CD44 with ERM proteins. *J Biol Chem* **279:** 11898-11905.

Jones, T.A., Zou,J.-Y., Cowan,S.W. and Kjeldgaard,M. 1991. Improved methods for building protein models in electron density maps and the location of errors in these models. *Acta Crystallogr. A,* **47:** 110-119.

Kajita, M., Itoh, Y., Chiba, T., Mori, H., Okada, A., Kinoh, H., and Seiki, M. 2001. Membrane-type 1 matrix metalloproteinase cleaves CD44 and promotes cell migration. *J Cell Biol* **153:** 893-904.

Kotani, H., Takaishi, K., Sasaki, T., and Takai, Y. 1997. Rho regulates association of both the ERM family and vinculin with the plasma membrane in MDCK cells. *Oncogene* **14:** 1705-1713.

Laskowski, R.A., MacArthur,M.W., Moss,D.S. and Thornton,J.M. 1993. PROCHECK: a program to check the stereochemical quality of protein structures. *J. Appl. Crystallogr.,* **26:** 283-291.

Legg, J.W., and Isacke, C.M. 1998. Identification and functional analysis of the ezrin-binding site in the hyaluronan receptor, CD44. *Curr Biol* **8:** 705-708.

Li, Q., Nance, M.R., Kulikauskas, R., Nyberg, K., Fehon, R., Karplus, P.A., Bretscher, A., and Tesmer, J.J. 2007. Self-masking in an Intact ERM-merlin Protein: An Active Role for the Central alpha-Helical Domain. *J Mol Biol* **365:** 1446-1459.

Lichtenthaler, S.F., Dominguez, D.I., Westmeyer, G.G., Reiss, K., Haass, C., Saftig, P., De Strooper, B., and Seed, B. 2003. The cell adhesion protein P-selectin glycoprotein ligand-1 is a substrate for the aspartyl protease BACE1. *J Biol Chem* **278:** 48713-48719.

Lozupone, F., Lugini, L., Matarrese, P., Luciani, F., Federici, C., Iessi, E., Margutti, P., Stassi, G., Malorni, W., and Fais, S. 2004. Identification and relevance of the CD95-binding domain in the N-terminal region of ezrin. *J Biol Chem* **279:** 9199-9207.

Maemura, K., and Fukuda, M. 1992. Poly-N-acetyllactosaminyl O-glycans attached to leukosialin. The presence of sialyl Le(x) structures in O-glycans. *J Biol Chem* **267:** 24379-24386.

Magendantz, M., Henry, M.D., Lander, A., and Solomon, F. 1995. Interdomain interactions of radixin in vitro. *J Biol Chem* **270:** 25324-25327.

Mangeat, P., Roy, C., and Martin, M. 1999. ERM proteins in cell adhesion and membrane dynamics. *Trends Cell Biol* **9:** 187-192.

Matsui, T., Maeda, M., Doi, Y., Yonemura, S., Amano, M., Kaibuchi, K., Tsukita, S., and Tsukita, S. 1998. Rho-kinase phosphorylates COOH-terminal threonines of ezrin/radixin/moesin (ERM) proteins and regulates their head-to-tail association. *J Cell Biol* **140:** 647-657.

Matsui, T., Yonemura, S., Tsukita, S., and Tsukita, S. 1999. Activation of ERM proteins in vivo by Rho involves phosphatidyl-inositol 4-phosphate 5-kinase and not ROCK kinases. *Curr Biol* **9:** 1259-1262.

Matthews, B.W. 1968. Solvent content of protein crystals. *J Mol Biol* **33:** 491-497.

McEver, R.P., and Cummings, R.D. 1997. Perspectives series: cell adhesion in vascular biology. Role of PSGL-1 binding to selectins in leukocyte recruitment. *J Clin Invest* **100:** 485-491.

Montoya, M.C., Sancho, D., Bonello, G., Collette, Y., Langlet, C., He, H.T., Aparicio, P., Alcover, A., Olive, D., and Sanchez-Madrid, F. 2002. Role of ICAM-3 in the initial interaction of T lymphocytes and APCs. *Nat Immunol* **3:** 159-168.

Ng, T., Parsons, M., Hughes, W.E., Monypenny, J., Zicha, D., Gautreau, A., Arpin, M., Gschmeissner, S., Verveer, P.J., Bastiaens, P.I., et al. 2001. Ezrin is a downstream effector of trafficking PKC-integrin complexes involved in the control of cell motility. *Embo J* **20:** 2723-2741.

Otwinowski, Z.a.M., W. 1997. Processing of X-ray diffraction data collected in oscillation mode.

In Methods Enzymol. **276:** 307-326.

Pearson, M.A., Reczek, D., Bretscher, A., and Karplus, P.A. 2000. Structure of the ERM protein moesin reveals the FERM domain fold masked by an extended actin binding tail domain. *Cell* **101:** 259-270.

Pedraza-Alva, G., Merida, L.B., Burakoff, S.J., and Rosenstein, Y. 1998. T cell activation through the CD43 molecule leads to Vav tyrosine phosphorylation and mitogen-activated protein kinase pathway activation. *J Biol Chem* **273:** 14218-14224.

Perkins, S.J. 1986. Protein volumes and hydration effects. The calculations of partial specific volumes, neutron scattering matchpoints and 280-nm absorption coefficients for proteins and glycoproteins from amino acid sequences. *Eur J Biochem* **157:** 169-180.

Pietromonaco, S.F., Simons, P.C., Altman, A., and Elias, L. 1998. Protein kinase C-theta phosphorylation of moesin in the actin-binding sequence. *J Biol Chem* **273:** 7594-7603.

Reczek, D., Berryman, M., and Bretscher, A. 1997. Identification of EBP50: A PDZ-containing phosphoprotein that associates with members of the ezrin-radixin-moesin family. *J Cell Biol* **139:** 169-179.

Reczek, D., and Bretscher, A. 1998. The carboxyl-terminal region of EBP50 binds to a site in the amino-terminal domain of ezrin that is masked in the dormant molecule. *J Biol Chem* **273:** 18452-18458.

Ren, X.D., Bokoch, G.M., Traynor-Kaplan, A., Jenkins, G.H., Anderson, R.A., and Schwartz, M.A. 1996. Physical association of the small GTPase Rho with a 68-kDa phosphatidylinositol 4-phosphate 5-kinase in Swiss 3T3 cells. *Mol Biol Cell* **7:** 435-442.

Ren, X.D., and Schwartz, M.A. 1998. Regulation of inositol lipid kinases by Rho and Rac. *Curr Opin Genet Dev* **8:** 63-67.

Sainio, M., Zhao, F., Heiska, L., Turunen, O., den Bakker, M., Zwarthoff, E., Lutchman, M.,

Rouleau, G.A., Jaaskelainen, J., Vaheri, A., et al. 1997. Neurofibromatosis 2 tumor suppressor protein colocalizes with ezrin and CD44 and associates with actin-containing cytoskeleton. *J Cell Sci* **110 (Pt 18):** 2249-2260.

Schuck, P. 2000. Size-distribution analysis of macromolecules by sedimentation velocity ultracentrifugation and lamm equation modeling. *Biophys J* **78:** 1606-1619.

Serrador, J.M., Alonso-Lebrero, J.L., del Pozo, M.A., Furthmayr, H., Schwartz-Albiez, R., Calvo, J., Lozano, F., and Sanchez-Madrid, F. 1997. Moesin interacts with the cytoplasmic region of intercellular adhesion molecule-3 and is redistributed to the uropod of T lymphocytes during cell polarization. *J Cell Biol* **138:** 1409-1423.

Serrador, J.M., Nieto, M., Alonso-Lebrero, J.L., del Pozo, M.A., Calvo, J., Furthmayr, H., Schwartz-Albiez, R., Lozano, F., Gonzalez-Amaro, R., Sanchez-Mateos, P., et al. 1998. CD43 interacts with moesin and ezrin and regulates its redistribution to the uropods of T lymphocytes at the cell-cell contacts. *Blood* **91:** 4632-4644.

Shaw, R.J., Henry, M., Solomon, F., and Jacks, T. 1998. RhoA-dependent phosphorylation and relocalization of ERM proteins into apical membrane/actin protrusions in fibroblasts. *Mol Biol Cell* **9:** 403-419.

Shimizu, T., Seto, A., Maita, N., Hamada, K., Tsukita, S., Tsukita, S., and Hakoshima, T. 2002. Structural basis for neurofibromatosis type 2. Crystal structure of the merlin FERM domain. *J Biol Chem* **277:** 10332-10336.

Simons, P.C., Pietromonaco, S.F., Reczek, D., Bretscher, A., and Elias, L. 1998. C-terminal threonine phosphorylation activates ERM proteins to link the cell's cortical lipid bilayer to the cytoskeleton. *Biochem Biophys Res Commun* **253:** 561-565.

Takahashi, K., Sasaki, T., Mammoto, A., Hotta, I., Takaishi, K., Imamura, H., Nakano, K., Kodama, A., and Takai, Y. 1998. Interaction of radixin with Rho small G protein GDP/GTP exchange protein Dbl. *Oncogene* **16:** 3279-3284.

Takahashi, K., Sasaki, T., Mammoto, A., Takaishi, K., Kameyama, T., Tsukita, S., and Takai,

Y. 1997. Direct interaction of the Rho GDP dissociation inhibitor with ezrin/radixin/moesin initiates the activation of the Rho small G protein. *J Biol Chem* **272:** 23371-23375.

Terawaki, S., Maesaki, R., and Hakoshima, T. 2006. Structural basis for NHERF recognition by ERM proteins. *Structure* **14:** 777-789.

Tran Quang, C., Gautreau, A., Arpin, M., and Treisman, R. 2000. Ezrin function is required for ROCK-mediated fibroblast transformation by the Net and Dbl oncogenes. *Embo J* **19:** 4565-4576.

Tsukita, S., Oishi, K., Sato, N., Sagara, J., Kawai, A., and Tsukita, S. 1994. ERM family members as molecular linkers between the cell surface glycoprotein CD44 and actin-based cytoskeletons. *J Cell Biol* **126:** 391-401.

Tsukita, S., and Yonemura, S. 1999. Cortical actin organization: lessons from ERM (ezrin/radixin/moesin) proteins. *J Biol Chem* **274:** 34507-34510.

Uhlik, M.T., Temple, B., Bencharit, S., Kimple, A.J., Siderovski, D.P., and Johnson, G.L. 2005. Structural and evolutionary division of phosphotyrosine binding (PTB) domains. *J Mol Biol* **345:** 1-20.

Urzainqui, A., Serrador, J.M., Viedma, F., Yanez-Mo, M., Rodriguez, A., Corbi, A.L., Alonso-Lebrero, J.L., Luque, A., Deckert, M., Vazquez, J., et al. 2002. ITAM-based interaction of ERM proteins with Syk mediates signaling by the leukocyte adhesion receptor PSGL-1. *Immunity* **17:** 401-412.

Voltz, J.W., Weinman, E.J., and Shenolikar, S. 2001. Expanding the role of NHERF, a PDZ-domain containing protein adapter, to growth regulation. *Oncogene* **20:** 6309-6314.

Wang, W., Link, V., and Green, J.M. 2000. Identification and cloning of a CD43-associated serine/threonine kinase. *Cell Immunol* **205:** 34-39.

Yonemura, S., Hirao, M., Doi, Y., Takahashi, N., Kondo, T., and Tsukita, S. 1998.

Ezrin/radixin/moesin (ERM) proteins bind to a positively charged amino acid cluster in the juxta-membrane cytoplasmic domain of CD44, CD43, and ICAM-2. *J Cell Biol* **140:** 885-895.

Yonemura, S., Matsui, T., Tsukita, S., and Tsukita, S. 2002. Rho-dependent and -independent activation mechanisms of ezrin/radixin/moesin proteins: an essential role for polyphosphoinositides in vivo. *J Cell Sci* **115:** 2569-2580.

Yonemura, S., Nagafuchi, A., Sato, N., and Tsukita, S. 1993. Concentration of an integral membrane protein, CD43 (leukosialin, sialophorin), in the cleavage furrow through the interaction of its cytoplasmic domain with actin-based cytoskeletons. *J Cell Biol* **120:** 437-449.

Yonemura, S., Tsukita, S., and Tsukita, S. 1999. Direct involvement of ezrin/radixin/moesin (ERM)-binding membrane proteins in the organization of microvilli in collaboration with activated ERM proteins. *J Cell Biol* **145:** 1497-1509.

Yun, C.H., Lamprecht, G., Forster, D.V., and Sidor, A. 1998. NHE3 kinase A regulatory protein E3KARP binds the epithelial brush border Na+/H+ exchanger NHE3 and the cytoskeletal protein ezrin. *J Biol Chem* **273:** 25856-25863.

6 Acknowledgments

I would like to thank my supervisor, Prof. Toshio Hakoshima (Nara Institute of Science and Technology), for teaching me protein crystallography, for his guidance, and support in the past five years.

I would like to thank Dr. Ken Kitano (Nara Institute of Science and Technology) for a lot of practical advices for protein crystallographic studies during all my work.

I would like to thank Dr. Sachiko Tsukita (Faculty of Medicine, Kyoto University, and College of Medical Technology) and Dr. Shoichiro Tsukita (Faculty of Medicine, Kyoto University) for providing us the expression vectors of the radixin FERM domain and CD43, and the precious discussions.

I also wish to thank Dr. Ryoko Maesaki (Nara Institute of Science and Technology), Dr. Shigeru Sakurai (Nara Institute of Science and Technology), Dr. Shinichi Terawaki (Nara Institute of Science and Technology), Dr. Hiroto Yamaguchi (Institute for protein research, Osaka university) for a lot of advices and support for my studies.

I wish to thank Junko Tsukamoto for her technical support in performing MALDI-TOF-MS and the N-terminal analysis.

Finally, I wish to thank colleagues, all the members of our laboratory for support during these five years.

Yumiko Takai

February 1, 2007